INTRODUCTION TO RADIOLOGICAL PHYSICS AND RADIATION DOSIMETRY

FRANK HERBERT ATTIX
Professor of Medical Physics
University of Wisconsin Medical School
Madison, Wisconsin

A Wiley-Interscience Publication
JOHN WILEY & SONS
New York Chichester Brisbane Toronto Singapore

CHAPTER 7

Gamma- and X-Ray Interactions in Matter

I. INTRODUCTION

There are five types of interactions with matter by x- and γ-ray photons which must be considered in radiological physics:

1. Compton effect
2. Photoelectric effect
3. Pair production
4. Rayleigh (coherent) scattering
5. Photonuclear interactions

The first three of these are the most important, as they result in the transfer of energy to electrons, which then impart that energy to matter in many (usually small) Coulomb-force interactions along their tracks. Rayleigh scattering is elastic; the photon is merely redirected through a small angle with no energy loss. Photonuclear interactions are only significant for photon energies above a few MeV, where they may create radiation-protection problems through the (γ, n) production of neutrons and consequent radioactivation.

The relative importance of Compton effect, photoelectric effect, and pair production depends on both the photon quantum energy ($E_\gamma = h\nu$) and the atomic number Z of the absorbing medium. Figure 7.1 indicates the regions of Z and E_γ in which each interaction predominates. The curves show where two kinds of interactions are equally probable. It will be seen that the photoelectric effect is dominant at the lower

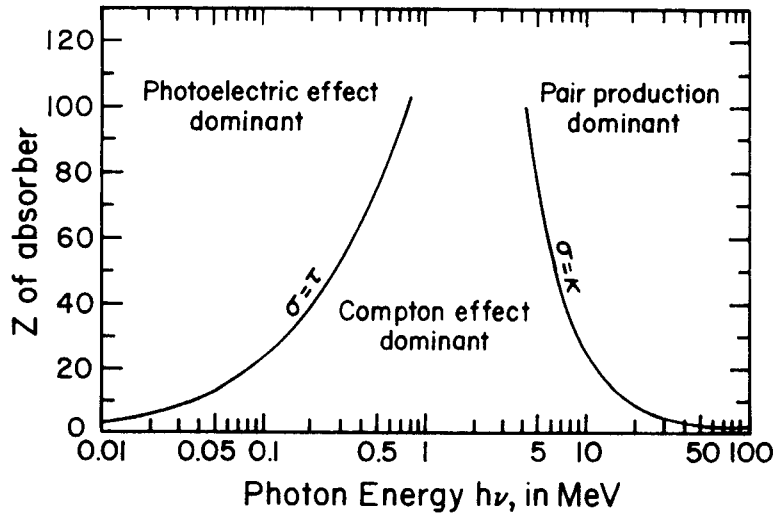

FIGURE 7.1. Relative importance of the three major types of γ-ray interactions. The curves show the values of Z and E_γ for which two types of effects are equal. (Reproduced from Evans (1955) with permission of R.D. Evans and McGraw-Hill Book Company.)

photon energies, the Compton effect takes over at medium energies, and pair production at the higher energies. For low-Z media (e.g., carbon, air, water, human tissue) the region of Compton-effect dominance is very broad, extending from $\cong 20$ keV to $\cong 30$ MeV. This gradually narrows with increasing Z.

In this chapter each of the five kinds of interactions will be discussed, identifying their respective contributions to the coefficients for attenuation (μ/ρ), energy transfer (μ_{tr}/ρ), and energy absorption (μ_{en}/ρ).

II. COMPTON EFFECT

A description of the Compton effect can be conveniently subdivided into two aspects: *kinematics* and *cross section*. The first relates the energies and angles of the participating particles when a Compton event occurs; the second predicts the probability that a Compton interaction will occur. In both respects it is customary to assume that the electron struck by the incoming photon is initially *unbound* and *stationary*. These assumptions are certainly not rigorous, inasmuch as the electrons all occupy various atomic energy levels, thus are in motion and are bound to the nucleus. Nevertheless the resulting errors remain inconsequential in radiological physics applications, because of the dominance of the competing photoelectric effect under the conditions (high Z, low $h\nu$) where electron binding effects are the most important in Compton interactions.

In the present chapter the initial motion and binding of the electron will be ignored. The Klein–Nishina treatment of the cross section, to be presented in Section II.B.2, is based on free electrons, and Appendix D.1 tabulates K-N interaction, scattering, and energy-transfer cross sections in units of cm^2/electron, which are applicable to all elements under the zero-binding assumption. Discussion of the influence of electron binding on the Compton effect has been given by Hubbell et al., (1980), Johns and Cunningham (1983), and Anderson (1984).

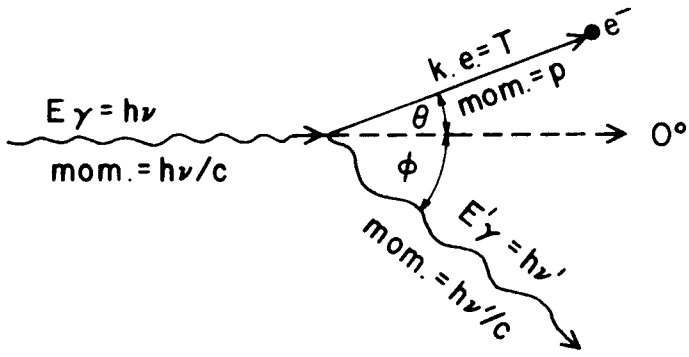

FIGURE 7.2. Kinematics of the Compton effect. A photon of quantum energy $h\nu$ incident from the left strikes an unbound stationary electron, scattering it at angle θ relative to the incident photon's direction, with kinetic energy T. The scattered photon $h\nu'$ departs at angle φ on the opposite side of the original direction, in the same scattering plane. Energy and momentum are each conserved. The assumption of an unbound electron means that the above kinematic relationships are independent of the atomic number of the medium.

A. Kinematics

Figure 7.2 schematically shows a photon of energy $h\nu$ colliding with an electron. The photon's incident forward momentum is $h\nu/c$, where c is the speed of light in vacuum. The stationary target electron has no initial kinetic energy or momentum.

After the collision the electron departs at angle θ, with kinetic energy T and momentum p. The photon scatters at angle φ with a new, lower quantum energy $h\nu'$ and momentum $h\nu'/c$. The solution to the collision kinetics is based upon conservation of both energy and momentum. Energy conservation requires that

$$T = h\nu - h\nu' \tag{7.1}$$

Conservation of momentum along the original photon direction (0°) can be expressed as

$$\frac{h\nu}{c} = \frac{h\nu'}{c} \cos \varphi + p \cos \theta$$

or

$$h\nu = h\nu' \cos \varphi + pc \cos \theta \tag{7.2}$$

Conservation of momentum perpendicular to the direction of incidence gives the equation

$$h\nu' \sin \varphi = pc \sin \theta \tag{7.3}$$

pc can be written in terms of T in Eqs. (7.2) and (7.3) by invoking the "law of invariance":

$$pc = \sqrt{T(T + 2\, m_0c^2)} \tag{7.4}$$

in which m_0 is the electron's rest mass. This equation can be derived from the following three relativistic relationships:

$$m = \frac{m_0}{\sqrt{1 - (v/c)^2}} \tag{7.5}$$

$$T = mc^2 - m_0c^2 \tag{7.6}$$

$$p = mv \tag{7.7}$$

where v is the electron's velocity, m is its relativistic mass, and p its momentum.

As a result of the substitution for pc, Eqs. (7.1), (7.2), and (7.3) constitute a set of three simultaneous equations in these five parameters: $h\nu$, $h\nu'$, T, θ, and φ. These equations can be solved algebraically to obtain any three of the variables we choose in a single equation. Of the many equations that may be thus derived, the following set of three equations, each in three variables, provides in convenient form a complete solution to the kinematics of Compton interactions:

$$h\nu' = \frac{h\nu}{1 + (h\nu/m_0c^2)(1 - \cos\varphi)} \tag{7.8}$$

$$T = h\nu - h\nu' \tag{7.9}$$

$$\cot\theta = \left(1 + \frac{h\nu}{m_0c^2}\right)\tan\left(\frac{\varphi}{2}\right) \tag{7.10}$$

in which m_0c^2 (the rest energy of the electron) is 0.511 MeV, and $h\nu$, $h\nu'$ and T are also expressed in MeV.

It will be seen from Eq. (7.8) that for a given value of $h\nu$, the energy $h\nu'$ and angle φ of the scattered photon are uniquely correlated to each other. Equation (7.9) then provides the kinetic energy T of the corresponding scattered electron, and Eq. (7.10) gives its scattering angle θ.

Figure 7.3 is a simple graphical representation of the kinematic relationships between $h\nu$, $h\nu'$, and T, as expressed by Eqs. (7.8) and (7.9). It can be seen that for $h\nu$ smaller than about 0.01 MeV, all the curves for different φ-values converge along the diagonal, indicating that $h\nu' = h\nu$ regardless of photon scattering angle. Consequently the electron receives practically no kinetic energy in the interaction. This means that Compton scattering is nearly elastic for low photon energies. An earlier theory of γ-ray scattering by Thomson, based on observations only at low energies, predicted that the scattered photon should always have the same energy as the incident one, regardless of $h\nu$ or φ. That is shown in Fig. 7.3 by the extension of the diagonal line to high energies. This curve also applies to the Compton effect for the trivial case of straight-ahead scattering, $\varphi = 0$.

The failure of the Thomson theory (see next section) to describe high-energy photon scattering necessitated the development of Compton's theory, which provides the other curves in Fig. 7.3 for the representative photon scattering angles $\varphi = 45°$, $90°$, and $180°$. For high-energy incident photons the backscattered photon ($\varphi = 180°$) has an energy $h\nu'$ approaching 0.2555 MeV, while side-scattered photons ($\varphi = 90°$) have $h\nu' \rightarrow 0.511$ MeV.

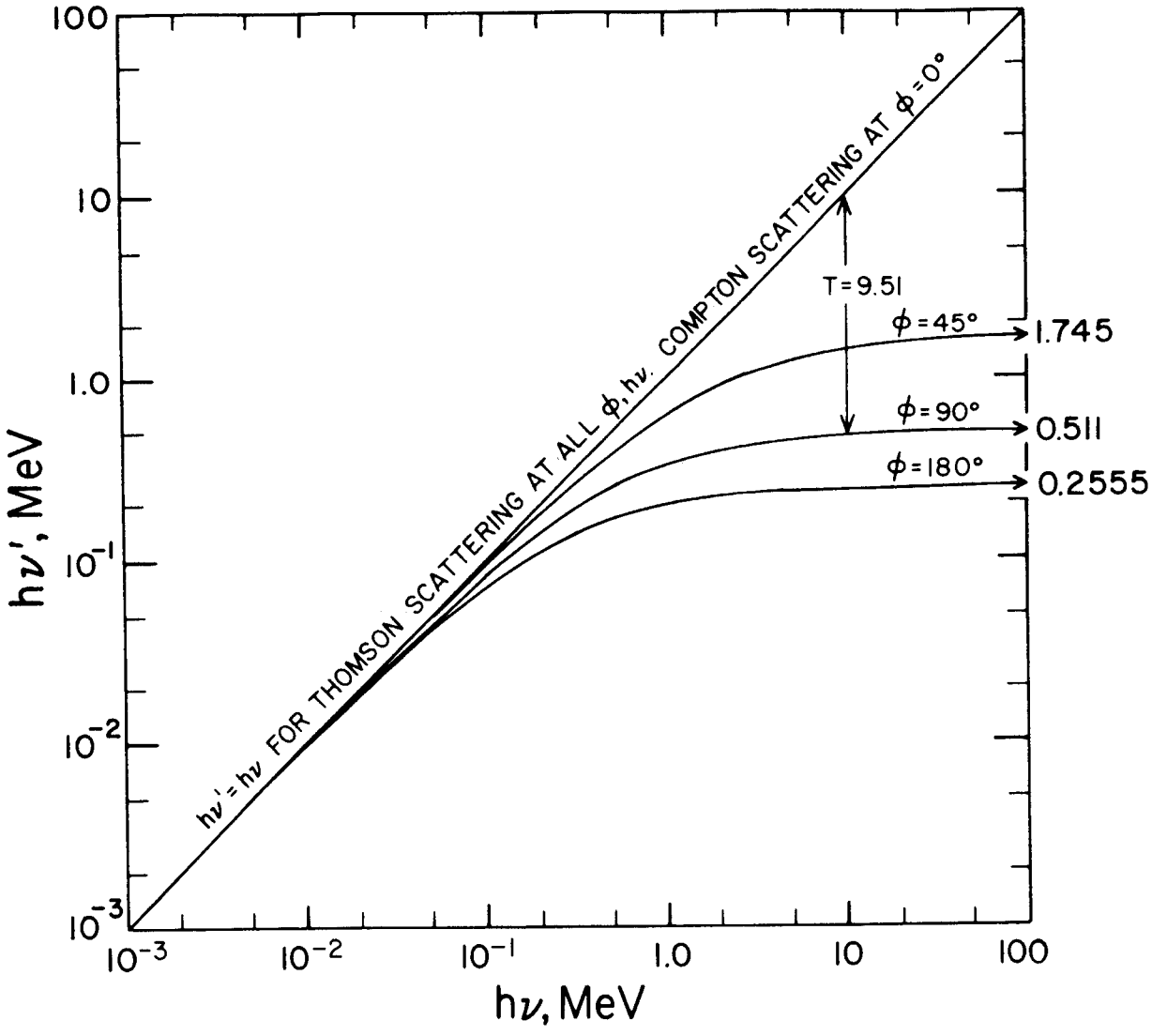

FIGURE 7.3. Graphical representation of the kinematic relationship of $h\nu$, $h\nu'$, and T in the Compton effect, as described by Eqs. (7.8) and (7.9). Curves are shown only for $\varphi = 0$, 45°, 90° and 180°. Note that T is to be interpreted as the vertical separation of any φ-curve from the $\varphi = 0$ diagonal. In the case shown ($h\nu = 10$ MeV, $\varphi = 90°$), $T = 9.51$ MeV.

The kinetic energy of the recoiling electron is given graphically in Fig. 7.3 as the vertical distance of the curve for the appropriate φ below the diagonal line, in terms of energy on the $h\nu'$ scale. Thus for the example shown by the arrow ($h\nu = 10$ MeV and $\varphi = 90°$), $T = 10 - 0.49 = 9.51$ MeV. For backscattering of photons, the electron is projected forward ($\theta = 0$) with an energy equal to $h\nu - h\nu'$, which approaches $h\nu - 0.2555$ MeV for very large $h\nu$. The photon is evidently able to transfer most of its energy to the electron in that case, but can never give away all of its energy in a Compton collision with a free electron.

Figure 7.4 contains graphs of the relationship between φ, θ, and $h\nu$ as given by Eq. (7.10), for several values of $h\nu$. When $\varphi = 0$, $\theta = 90°$, and when $\varphi = 180°$, $\theta = 0°$, for all photon energies. Obviously the electron can only be scattered in the forward hemisphere by a Compton event. The dependence of θ upon φ is a strong function of $h\nu$ between the angular extremes. For low photon energies $\theta \cong 90° -$

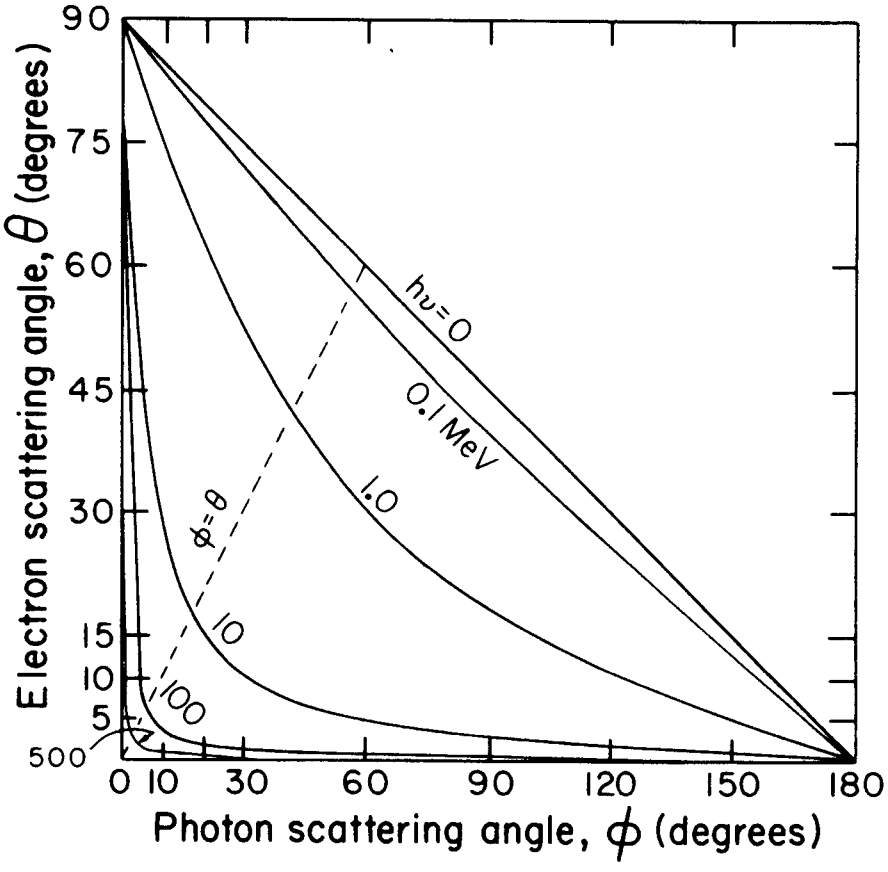

FIGURE 7.4. Relationship of the electron scattering angle θ to the photon scattering angle φ in the Compton effect, from Eq. (7.10). Curves are shown for the incident photon energies 0, 0.1, 1.0, 10, 100, and 500 MeV. The dashed line is the locus where $\theta = \varphi$, when the electron and photon are scattered at equal angles on opposite sides of the incident photon's direction.

$\varphi/2$; the electron scattering angle gradually decreases from 90° to 0° as the photon angle increases from 0° to 180°, and $\theta = \varphi$ at about 60°. At high photon energies the major variation in θ is concentrated at small φ-values, and vice versa. For example, at $h\nu = 500$ MeV, $\theta = \varphi$ at 2.59°. All photons scattered at angles between 2.59° and 180° are kinematically related to the electrons scattered forward at angles $\theta < 2.59°$. All electrons scattered at angles θ between 2.59° and 90° are likewise related to the photons scattered forward between 0 and 2.59°.

It is important to remember that Figs. 7.3 and 7.4 and Eqs. (7.8), (7.9), and (7.10) tell us nothing about the *probability* of a photon or an electron being Compton-scattered in any particular direction; that is a separate matter to be discussed in Section II.B. The foregoing figures and equations only state how the various parameters must be related to each other if a Compton interaction does occur.

B. Interaction Cross Section for the Compton Effect

1. THOMSON SCATTERING

J. J. Thomson provided the earliest theoretical description of the process by which a γ-ray photon can be scattered by an electron (see Evans, 1955). In this theory the electron was assumed to be free to oscillate under the influence of the electric vector

of an incident classical electromagnetic wave, then promptly to reemit a photon of the same energy. The electron thus retains no kinetic energy as a result of this elastic scattering event. This agrees with the kinematic predictions of the later relativistic Compton treatment quite well up to about $h\nu = 0.01$ MeV, for which Eq. (7.8) gives $h\nu' = 0.0096$ MeV. Figure 7.3 clearly shows this agreement at low photon energies.

Thomson also deduced that the differential cross section per electron for a photon scattered at angle φ, per unit solid angle, could be expressed as

$$\frac{d_e\sigma_0}{d\Omega_\varphi} = \frac{r_0^2}{2}(1 + \cos^2\varphi) \tag{7.11}$$

in typical units of $\text{cm}^2\ \text{sr}^{-1}$ per electron. $r_0 = e^2/m_0c^2 = 2.818 \times 10^{-13}$ cm is called the "classical electron radius". The value of Eq. (7.11) is $7.94 \times 10^{-26}\ \text{cm}^2\ \text{sr}^{-1}$ e^{-1} at $\varphi = 0$ and 180°, and half of that at $\varphi = 90°$. Thus the angular distribution of scattered photons for a large number of events is predicted to be front-back symmetrical, according to Thomson. If the beam of photons is unpolarized, there will also be cylindrical symmetry around the beam axis. The angular distribution of Thomson-scattered photons is approximated by the uppermost curve in Fig. 7.5, which was drawn to show the corresponding distribution of Compton-scattered photons for $h\nu = 0.01$ MeV. When $h\nu$ approaches zero, the two theories converge, as relativistic considerations become irrelevant.

The total Thomson scattering cross section per electron, ${}_e\sigma_0$, can be gotten by integrating Eq. (7.11) over all directions of scattering. This will be simplified by assuming cylindrical symmetry and integrating over $0 \leq \varphi \leq \pi$, noting that the annular element of solid angle is given in terms of φ by $d\Omega_\varphi = 2\pi \sin\varphi\, d\varphi$:

$$\begin{aligned} {}_e\sigma_0 &= \int_{\varphi=0}^{\pi} d_e\sigma_0 = \pi r_0^2 \int_{\varphi=0}^{\pi} (1 + \cos^2\varphi) \sin\varphi\, d\varphi \\ &= \frac{8\pi r_0^2}{3} = 6.65 \times 10^{-25}\ \text{cm}^2/\text{electron} \end{aligned} \tag{7.12}$$

This cross section (which can be thought of as an effective target area) is numerically equal to the probability of a Thomson-scattering event occurring when a single photon passes through a layer containing one electron per cm^2. It is also the fraction of a large number of incident photons that scatter in passing through the same layer, e.g., approximately 665 events for 10^{27} photons. So long as the fraction of photons interacting in a layer of matter by *all processes combined* remains less than about 0.05, the fraction may be assumed to be proportional to absorber thickness, i.e., the linear approximation is adequate. For greater thicknesses the exponential relation must be used (see Chapter 3).

More will be said about interaction cross sections for each kind of interaction later in the present chapter in discussing their contributions to μ_{tr}/ρ, μ_{en}/ρ, and the mass attenuation coefficient μ/ρ.

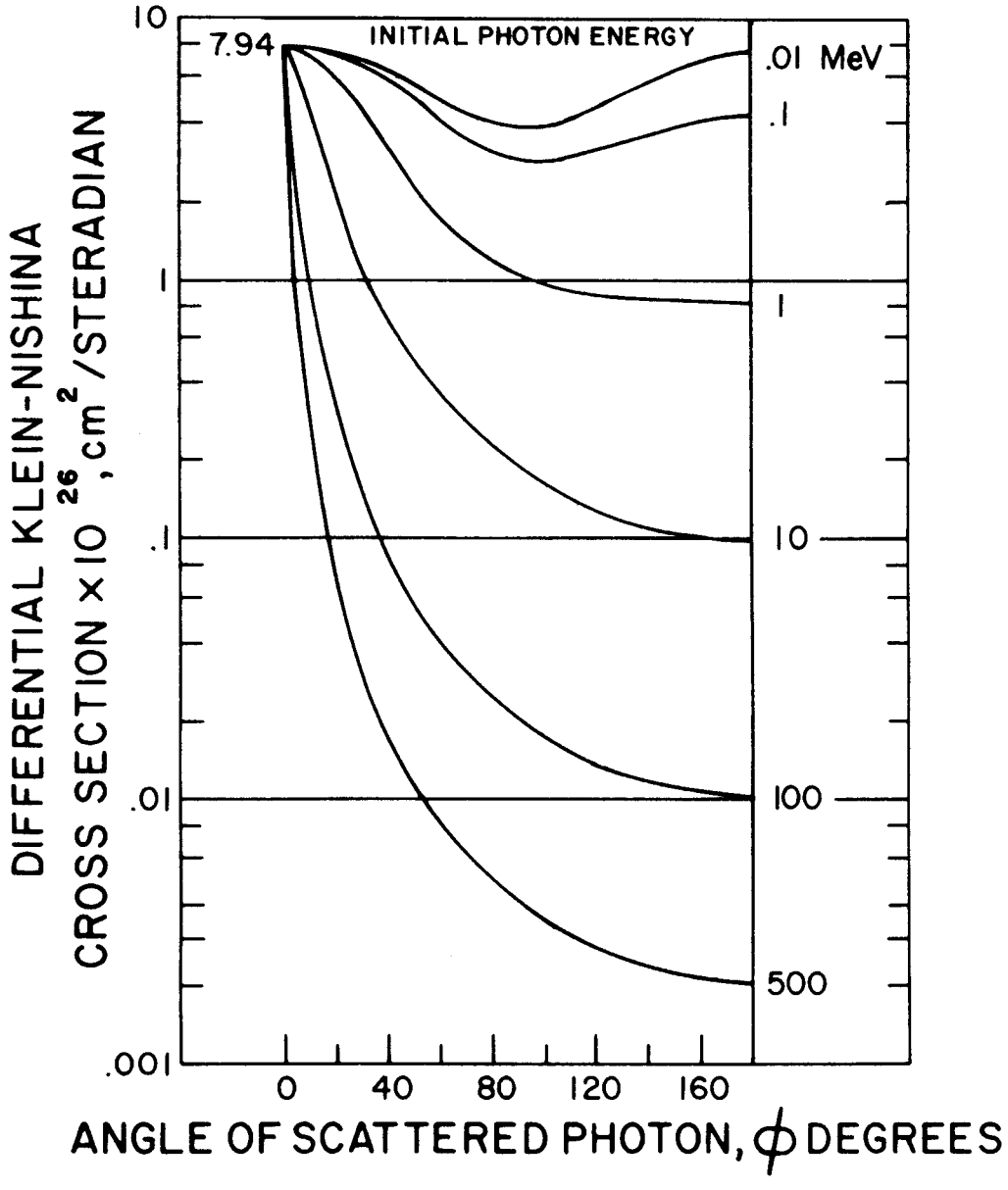

FIGURE 7.5. Differential Klein-Nishina cross section, $d_e\sigma/d\Omega_\varphi$ [see Eq. (7.13)] vs. angle φ of the scattered photon, for $h\nu$ = 0.01, 0.1, 1.0, 10, 100, and 500 MeV. This shows the angular distribution, per unit solid angle, of the scattered photons resulting from the Compton effect. (After Nelms, 1953.)

2. KLEIN–NISHINA CROSS SECTIONS FOR THE COMPTON EFFECT

In 1928 Klein and Nishina (see Evans, 1955) applied Dirac's relativistic theory of the electron to the Compton effect to obtain improved cross sections. Thomson's value of 6.65×10^{-25} cm$^2/e$, independent of $h\nu$, was known to be too large for $h\nu > 0.01$ MeV. The error reached a factor of 2 at $h\nu = 0.4$ MeV. The Klein-Nishina (K-N) treatment was remarkably successful in predicting the correct experimental value, even though they assumed unbound electrons, initially at rest. The differential cross section for photon scattering at angle φ, per unit solid angle and per electron, corresponding to Eq. (7.11) from Thomson's theory, may be written in the form

$$\frac{d_e\sigma}{d\Omega_\varphi} = \frac{r_0^2}{2}\left(\frac{h\nu'}{h\nu}\right)^2\left(\frac{h\nu}{h\nu'} + \frac{h\nu'}{h\nu} - \sin^2\varphi\right) \tag{7.13}$$

in which $h\nu'$ is given by Eq. (7.8). For low energies, as was previously pointed out, $h\nu' \cong h\nu$; hence Eq. (7.13) becomes

$$\frac{d_e\sigma}{d\Omega_\varphi} = \frac{r_0^2}{2}(2 - \sin^2\varphi) = \frac{r_0^2}{2}(1 + \cos^2\varphi) \tag{7.14}$$

which is identical to Eq. (7.11), verifying that the K-N differential cross section reduces to that of Thomson for the special case of low photon energies.

Figure 7.5 (Nelms, 1953) is a graphical representation of Eq. (7.13) for six values of $h\nu$. The forward bias of the scattered photons at high energies is apparent. That reference also contains eleven other carefully prepared graphs of $d_e\sigma/d\Omega_\varphi$ vs. φ for many intermediate energies, offering a very convenient display of Compton-effect data for purposes of estimation and hand calculation.*

The total K-N cross section per electron ($_e\sigma$) can be gotten from an integration of Eq. (7.13) over all photon scattering angles φ:

$$\begin{aligned}
{}_e\sigma &= 2\pi\int_{\varphi=0}^{\pi}\frac{d_e\sigma}{d\Omega_\varphi}\sin\varphi\,d\varphi \\
&= \pi r_0^2\int_0^{\pi}\left(\frac{h\nu'}{h\nu}\right)^2\left(\frac{h\nu}{h\nu'} + \frac{h\nu'}{h\nu} - \sin^2\varphi\right)\sin\varphi\,d\varphi \\
&= 2\pi r_0^2\left\{\frac{1+\alpha}{\alpha^2}\left[\frac{2(1+\alpha)}{1+2\alpha} - \frac{\ln(1+2\alpha)}{\alpha}\right] + \frac{\ln(1+2\alpha)}{2\alpha} - \frac{1+3\alpha}{(1+2\alpha)^2}\right\}
\end{aligned} \tag{7.15}$$

where $\alpha = h\nu/m_0c^2$, in which $h\nu$ is to be expressed in MeV and $m_0c^2 = 0.511$ MeV.

Equation (7.15) is shown graphically as the upper curve of Fig. 7.6. As expected, it is almost equal to the Thomson scattering cross section (6.65×10^{-25} cm^2/e) at $h\nu = 0.01$ MeV. It decreases gradually for higher photon energies to approach a ${}_e\sigma \propto (h\nu)^{-1}$ dependence.

It is important to remember that $_e\sigma$, which is tabulated in Appendix D.1, is independent of the atomic number Z:

$${}_e\sigma \propto Z^0 \tag{7.16}$$

since the electron binding energy has been assumed to be zero. Thus the K-N cross section per atom of any Z is given by

$${}_a\sigma = Z \cdot {}_e\sigma \qquad (\text{cm}^2/\text{atom}) \tag{7.17}$$

The corresponding K-N cross section per unit mass, σ/ρ, which is also called the Compton mass attenuation coefficient, is obtained from

*Nelms's report also has extensive families of curves of $h\nu'$ vs. φ, T vs. θ, $d_e\sigma/d\Omega_\theta$ vs. θ, $d_e\sigma/d(h\nu')$ vs. $h\nu'$, and $d\sigma/dT$ vs T. Note that Nelms' symbols differ from the present ones.

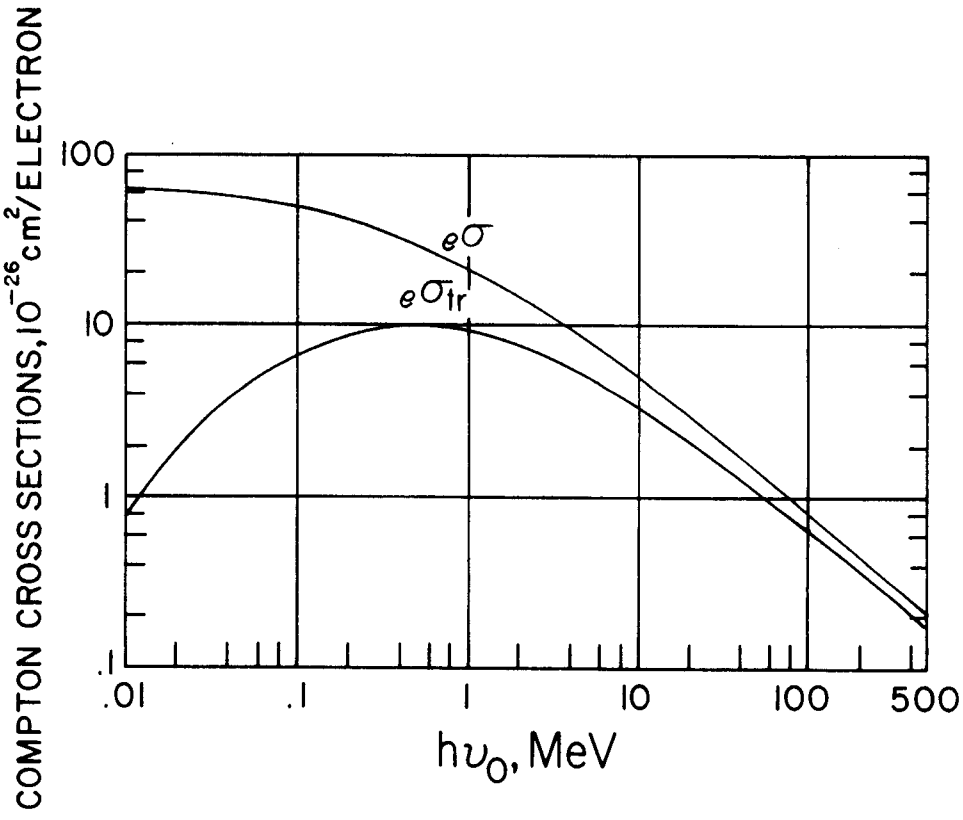

FIGURE 7.6. Klein–Nishina (Compton-effect) cross section per electron ($_e\sigma$) and corresponding energy-transfer cross section per electron ($_e\sigma_{tr}$) as a function of primary photon quantum energy $h\nu$. (After Nelms, 1953.)

$$\frac{\sigma}{\rho} = \frac{N_A Z}{A}\,{}_e\sigma \qquad (\text{cm}^2/\text{g}) \tag{7.18}$$

where $N_A = 6.022 \times 10^{23}$ mole^{-1} is Avogadro's constant, the number of atoms in a gram-atomic weight of any element or the number of molecules in a gram-molecular weight of any compound,

Z = number of electrons per atom of an element or per molecule of a compound,

A = number of grams per mole of material (i.e., A is the gram-atomic or molecular-weight),

ρ = density in g/cm^3, and

$N_A Z/A$ = number of electrons per gram of material.

Any interaction coefficient given in units of cm^2/g may of course be divided by 10 to convert it into units of m^2/kg.

Reviewing Eqs. 7.16–7.18 we see that $_e\sigma \propto Z^0$, $_a\sigma \propto Z$, and $\sigma/\rho \approx Z^0$, where the last, approximate proportionality requires some explanation: With the exception of hydrogen, for which $Z/A = 1$, Z/A ranges between 0.5 and 0.4, tending to decrease gradually with increasing Z (see Appendix B). The somewhat crude assumption of constant Z/A means that the Compton mass attenuation coefficient is approximately Z – independent, like the electronic cross section. The atomic cross section (7.17) is proportional to Z, *one power of Z greater than the others.* This latter pattern applies to

all interaction cross sections, even though their Z-dependence may differ from that of the Compton effect.

C. Energy-Transfer Cross Section for the Compton Effect

The total K–N cross section, multiplied by a unit thickness of 1 e/cm^2, also may be thought of as the fraction of the incident energy fluence, carried by a beam of many monoenergetic photons, that will be diverted into Compton interactions in passing through that layer of matter. In each interaction the energy of the incident photon ($h\nu$) is shared between the scattered photon ($h\nu'$) and the recoiling electron (T). It is of interest to know the overall fraction of $h\nu$ that is given to the electrons, averaged over all scattering angles, as this energy contributes to the kerma and thence to the dose. That is, we would like to know the value of $\overline{T}/h\nu$, where $\overline{T}$ is the average kinetic energy of the recoiling electrons. This can be obtained through first modifying the differential K–N cross section in Eq. (7.13) to obtain a quantity referred to as the differential K–N energy-transfer cross section, $d_e\sigma_{\text{tr}}/d\Omega_\varphi$:

$$\frac{d_e\sigma_{\text{tr}}}{d\Omega_\varphi} = \frac{d_e\sigma}{d\Omega_\varphi} \cdot \frac{T}{h\nu} = \frac{d_e\sigma}{d\Omega_\varphi} \cdot \frac{h\nu - h\nu'}{h\nu}$$

$$= \frac{r_0^2}{2}\left(\frac{h\nu'}{h\nu}\right)^2 \left(\frac{h\nu}{h\nu'} + \frac{h\nu'}{h\nu} - \sin^2\varphi\right)\left(\frac{h\nu - h\nu'}{h\nu}\right)$$

$$(\text{cm}^2\ \text{sr}^{-1}\ e^{-1}) \quad (7.19)$$

Integrating this over all photon scattering angles φ from 0 to 180°, as in Eq. (7.15), yields the following statement of ${}_e\sigma_{\text{tr}}$, the K–N energy-transfer cross section:

$${}_e\sigma_{\text{tr}} = 2\pi r_0^2 \left[\frac{2(1+\alpha)^2}{\alpha^2(1+2\alpha)} - \frac{1+3\alpha}{(1+2\alpha)^2} - \frac{(1+\alpha)(2\alpha^2 - 2\alpha - 1)}{\alpha^2(1+2\alpha)^2}\right.$$

$$\left. - \frac{4\alpha^2}{3(1+2\alpha)^3} - \left(\frac{1+\alpha}{\alpha^3} - \frac{1}{2\alpha} + \frac{1}{2\alpha^3}\right)\ln(1+2\alpha)\right]$$

$$(\text{cm}^2/e) \quad (7.20)$$

This cross section, multiplied by the unit thickness 1 e/cm^2, represents the fraction of the energy fluence in a monoenergetic photon beam that is diverted to the recoil electrons by Compton interactions in that layer. The Compton (or K–N) energy-transfer cross section is also plotted in Fig. 7.6 (lower curve). The vertical difference between the two curves represents the K–N cross section for the energy carried by the scattered photons, ${}_e\sigma_s$. Thus

$${}_e\sigma = {}_e\sigma_{\text{tr}} + {}_e\sigma_s \quad (7.21)$$

The average fraction of the incident photon's energy given to the electron is simply

$$\frac{\overline{T}}{h\nu} = \frac{{}_e\sigma_{\text{tr}}}{{}_e\sigma} \quad (7.22)$$

and one can obtain the average energy of the Compton recoil electrons generated by photons of energy $h\nu$ as

$$\overline{T} = h\nu \cdot \frac{{}_e\sigma_{tr}}{{}_e\sigma} \tag{7.23}$$

The ratios given in Eq. (7.22) are plotted in Fig. 7.7 on the basis of the data given in Fig. 7.6. At low energies the average fraction of $h\nu$ given to the electron approaches zero; for $h\nu = 1.6$ MeV the electrons get half, or $\overline{T} = 0.8$ MeV.

The contribution of the Compton effect to the photon mass attenuation coefficient μ/ρ is σ/ρ. The corresponding contribution to the mass energy-transfer coefficient is

$$\frac{\sigma_{tr}}{\rho} = \frac{N_A Z}{A} \cdot {}_e\sigma_{tr} \qquad (\text{cm}^2/\text{g}) \tag{7.24}$$

in reference to Eqs. (7.18) and (7.20).

The contributions of the several kinds of interactions to μ/ρ, μ_{tr}/ρ, and μ_{en}/ρ will be summarized in a later section.

Before proceeding to discussions of the other types of interactions, it will be helpful to show and explain two other useful forms of the differential K–N cross section that were included in the compilation by Nelms (1953). The first is $d_e\sigma/d\Omega_\theta$, the differential K–N cross section for electron scattering at angle θ, per unit solid angle and per electron. Note that the solid angle referred to in this case means that through which the *electron* scatters at angle θ. For $d_e\sigma/d\Omega_\varphi$ the solid angle is that through which the *photon* scatters at angle φ. The relationship between these two differential cross sections is

$$\frac{d_e\sigma}{d\Omega_\theta} = \frac{d_e\sigma}{d\Omega_\varphi} \cdot \frac{(1+\alpha)^2 (1-\cos\varphi)^2}{\cos^3\theta} \tag{7.25}$$

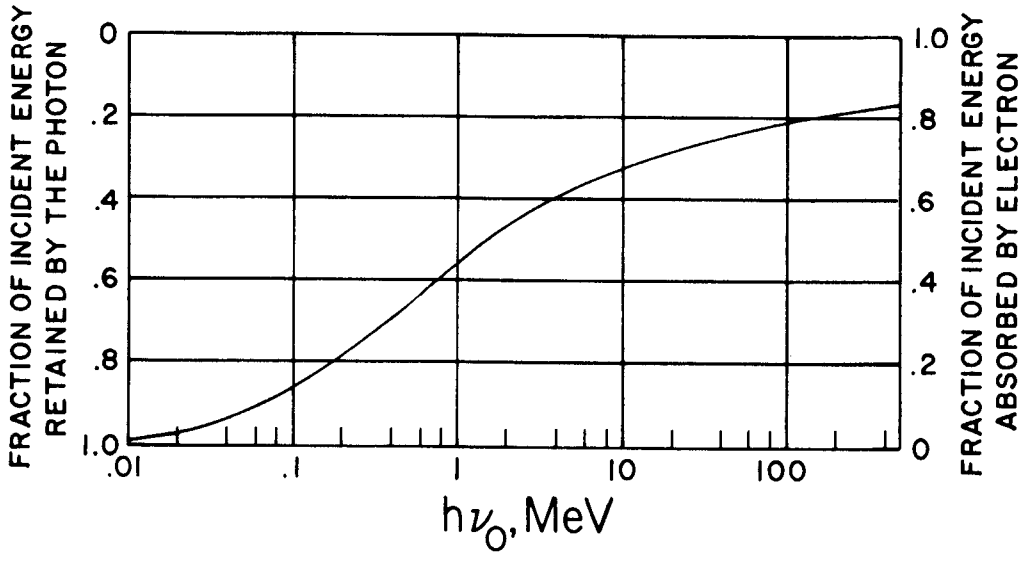

FIGURE 7.7. Mean fraction ($\overline{T}/h\nu$) of the incident photon's energy given to the recoiling electron in Compton interactions, averaged over all angles (right ordinate). Also, mean fraction ($h\overline{\nu}'/h\nu$) of energy retained by the scattered photon (left ordinate).

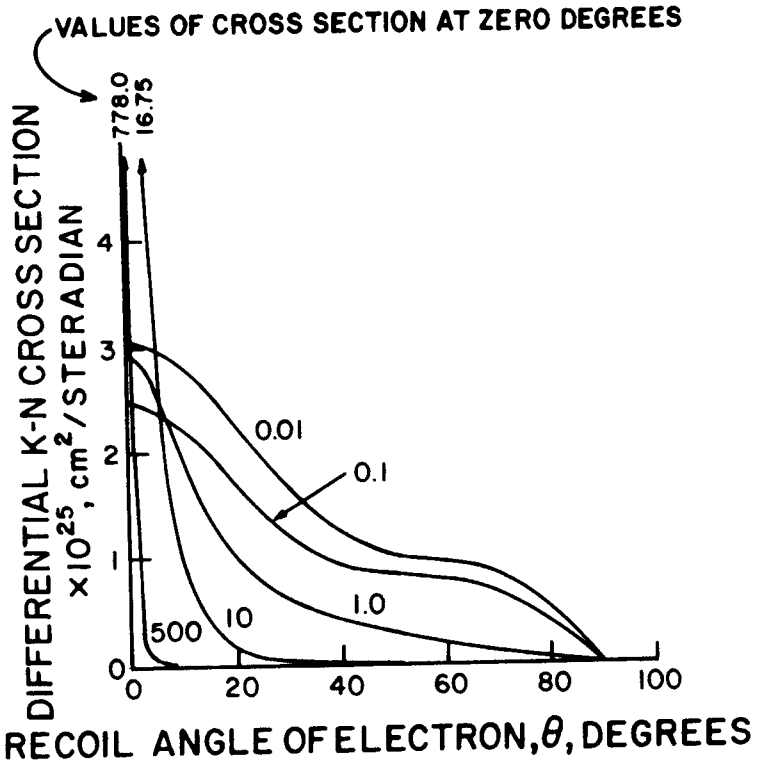

FIGURE 7.8. Differential Klein–Nishina cross section $d_e\sigma/d\Omega_\theta$, vs angle θ of the scattered electron for $h\nu$ = 0.01, 0.1, 1, 10, and 500 MeV. This shows the angular distribution, per unit solid angle, of the recoil electrons resulting from the Compton effect. (After Nelms, 1953.)

in which $d_e\sigma/d\Omega_\varphi$ is given by Eq. (7.13), and $\varphi = 2\tan^{-1}[(\cot\theta)/(1+\alpha)]$ from Eq. (7.10). Integration over all electron scattering angles from $\theta = 0$ to 90° must again give ${}_e\sigma$, as in Eq. (7.15).

Figure 7.8 displays Eq. (7.25) graphically for several values of $h\nu$, plotting $d_e\sigma/d\Omega_\theta$ vs. θ. The probability of electrons being scattered at $\theta = 90°$ approaches a constant value (zero) for all $h\nu$, while $d_e\sigma/d\Omega_\varphi = 7.94 \times 10^{-26}$ cm^2/sr e for all $h\nu$ at $\varphi = 0°$, as seen in Fig. 7.5. As the cross section decreases to $d_e\sigma/d\Omega_\varphi = 2 \times 10^{-29}$ cm^2/sr e for backscattered photons at $h\nu$ = 500 MeV (Fig. 7.5), the corresponding cross section for 0°-scattered electrons is seen from Fig. 7.8 to reach $d_e\sigma/d\Omega_\theta = 7.78 \times 10^{-23}$. This is an indication of how very strongly forward-directed the electrons become at high incident photon energies, while at the same time it becomes relatively unlikely that photons will be 180°-backscattered. This seems to be a paradox until one refers again to Fig. 7.4, in which it is evident that high-energy photons scattered at a wide range of angles must be associated with electrons recoiling at nearly 0°. The high forward momentum in the collision causes most of the electrons and most of the scattered photons to be strongly forward-directed when $h\nu$ is large.

The second additional form of differential K-N cross section that deserves mention here is $d_e\sigma/dT$, typically in cm^2 MeV^{-1} e^{-1}. This is the probability that a single photon will have a Compton interaction in traversing a layer containing one e/cm^2, transferring to that electron a kinetic energy between T and $T + dT$. Thus $d_e\sigma/dT$ is the energy distribution of the electrons, averaged over all scattering angles θ. It is given by the relation:

$$\frac{d_e\sigma}{dT} = \frac{\pi r_0^2 m_0 c^2}{(h\nu')^2} \times \left\{ \left[\frac{m_0 c^2 T}{(h\nu)^2} \right]^2 + 2 \left[\frac{h\nu'}{h\nu} \right]^2 + \frac{h\nu'}{(h\nu)^3} [(T - m_0 c^2)^2 - (m_0 c^2)^2] \right\} \quad (7.26)$$

Figure 7.9 is a graphical representation of Equation (7.26) for several values of $h\nu$. [Nelms (1953) gives families of curves also for many intermediate energies.] It is evident that the distribution of kinetic energies given to the Compton recoiling electrons tends to be fairly flat from zero almost up to the maximum electron energy, where a higher concentration occurs. As mentioned earlier in discussing Eqs. (7.8) and (7.9), the maximum electron energy T_{max} resulting from a head-on Compton collision ($\theta = 0°$) by a photon of energy $h\nu$ is $(h\nu - h\nu'_{min})$, which is equal to

$$T_{max} = \frac{2(h\nu)^2}{2h\nu + 0.511 \text{ MeV}} \quad (7.27)$$

This approaches $h\nu - 0.2555$ MeV for large hν. The higher concentration of electrons near this energy, as seen in Fig. 7.9, is consistent with the high probability of electron scattering near $\theta = 0°$, shown in Fig. 7.8. Both trends become more pronounced at high energies.

It should be remembered that the energy distributions shown in Fig. 7.9 are those occurring at production. The spectrum of Compton-electron energies present at a point in an extended medium under irradiation is generally degraded by the presence

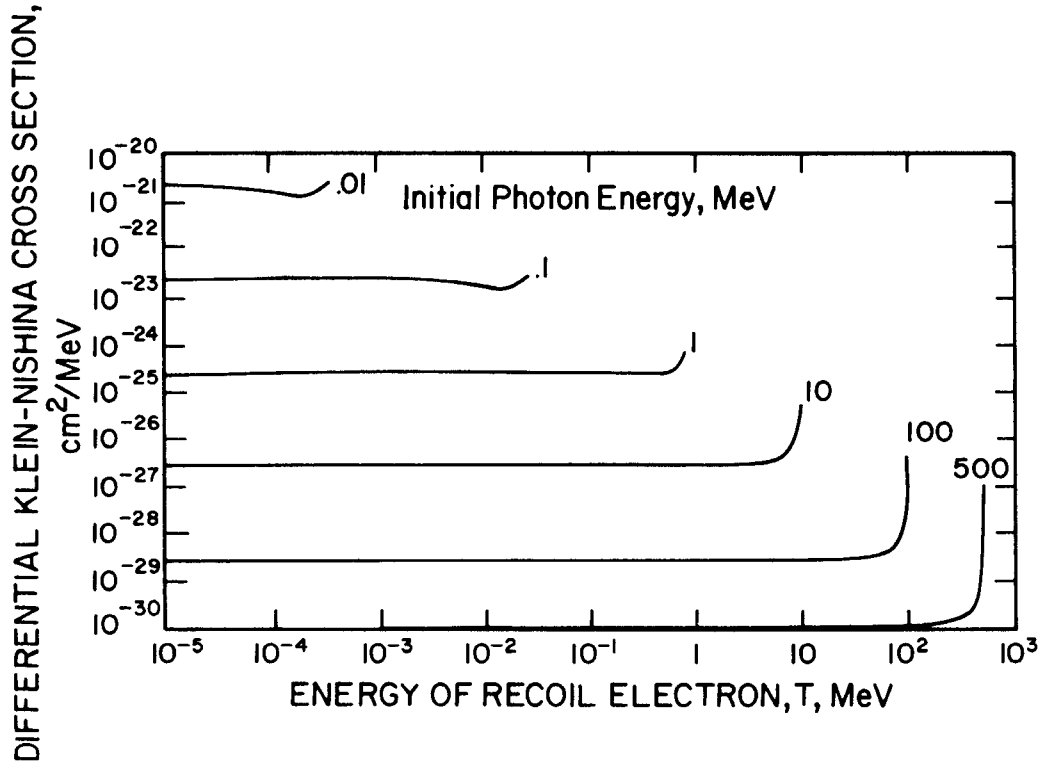

FIGURE 7.9. Differential Klein–Nishina cross section $d_e\sigma/dT$ expressing the initial energy spectrum of Compton recoiling electrons. (After Nelms, 1953.)

$$\frac{d_e\sigma}{dT} = \frac{\pi r_0^2 m_0 c^2}{(h\nu')^2} \times \left\{ \left[\frac{m_0 c^2 T}{(h\nu)^2} \right]^2 + 2 \left[\frac{h\nu'}{h\nu} \right]^2 + \frac{h\nu'}{(h\nu)^3} [(T - m_0 c^2)^2 - (m_0 c^2)^2] \right\} \quad (7.26)$$

Figure 7.9 is a graphical representation of Equation (7.26) for several values of $h\nu$. [Nelms (1953) gives families of curves also for many intermediate energies.] It is evident that the distribution of kinetic energies given to the Compton recoiling electrons tends to be fairly flat from zero almost up to the maximum electron energy, where a higher concentration occurs. As mentioned earlier in discussing Eqs. (7.8) and (7.9), the maximum electron energy T_{max} resulting from a head-on Compton collision ($\theta = 0°$) by a photon of energy $h\nu$ is $(h\nu - h\nu'_{min})$, which is equal to

$$T_{max} = \frac{2(h\nu)^2}{2h\nu + 0.511 \text{ MeV}} \quad (7.27)$$

This approaches $h\nu - 0.2555$ MeV for large hν. The higher concentration of electrons near this energy, as seen in Fig. 7.9, is consistent with the high probability of electron scattering near $\theta = 0°$, shown in Fig. 7.8. Both trends become more pronounced at high energies.

It should be remembered that the energy distributions shown in Fig. 7.9 are those occurring at production. The spectrum of Compton-electron energies present at a point in an extended medium under irradiation is generally degraded by the presence

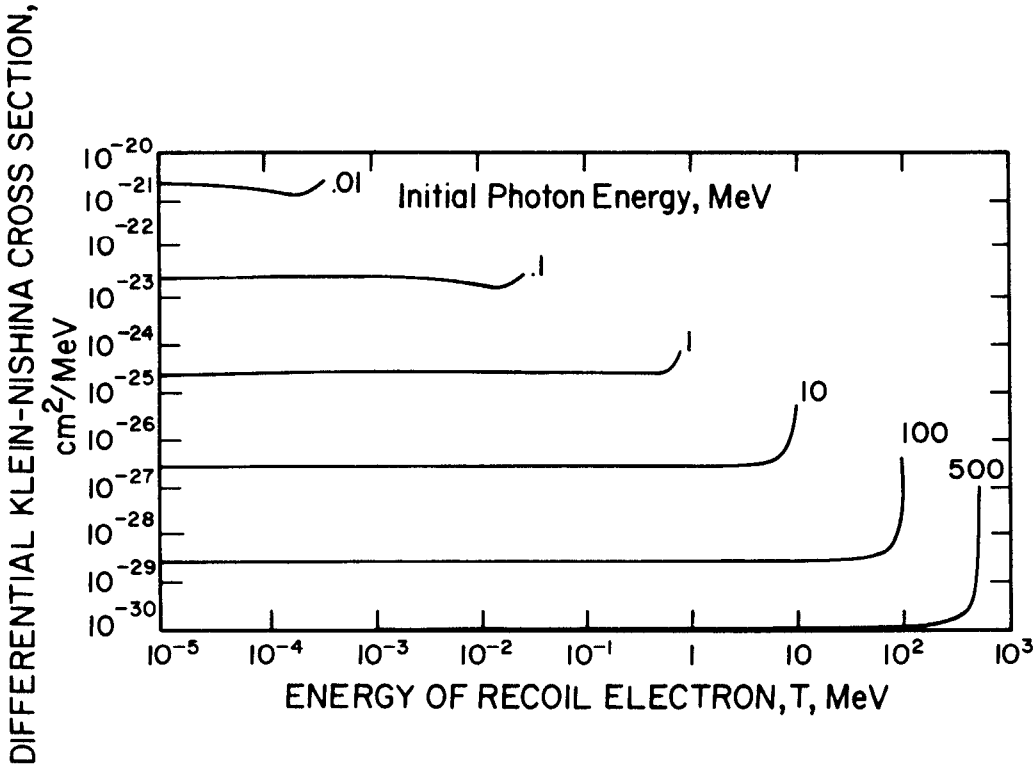

FIGURE 7.9. Differential Klein-Nishina cross section $d_e\sigma/dT$ expressing the initial energy spectrum of Compton recoiling electrons. (After Nelms, 1953.)

of electrons that have lost varying amounts of their energy depending on how far they have traveled through the medium. Under charged-particle equilibrium conditions this degraded electron energy distribution is called an "equilibrium spectrum." Such degraded spectra will be discussed in connection with cavity theory in Chapter 10.

Turner et al. (1980) and Todo et al. (1982) have provided useful spectra of electron starting energies resulting from monoenergetic photon interactions in water, calculated by the Monte Carlo method. They included contributions from the other interaction modes, in addition to Compton recoil-electron spectra.

III. PHOTOELECTRIC EFFECT

The photoelectric effect is the most important interaction of low-energy photons with matter, as indicated in Fig. 7.1. While the Compton effect's interaction cross section approaches a constant value, and its energy-transfer cross section diminishes as $h\nu$ decreases below 0.5 MeV (see Fig. 7.6), the corresponding cross sections for the photoelectric effect both increase strongly, especially for high-Z media. Consequently the photoelectric effect totally predominates over the Compton effect at low photon energies, particularly with respect to the energy transferred to secondary electrons.

A. Kinematics

It was seen in the case of the Compton effect that a photon cannot give up all of its energy in colliding with a free electron. However, it can do so in an encounter with a tightly bound electron, such as those in the inner shells of an atom, especially of high atomic number. This is called the photoelectric effect and is illustrated schematically in Fig. 7.10. An incident photon of quantum energy $h\nu$ is shown interacting with an atomic-shell electron bound by potential energy E_b. The photoelectric effect

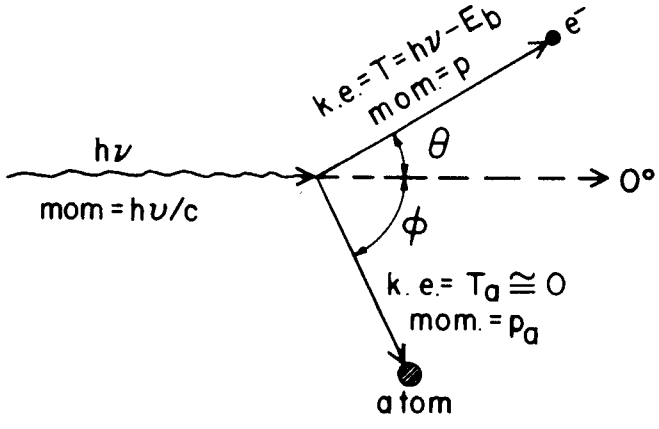

FIGURE 7.10. Kinematics of the photoelectric effect. A photon of quantum energy $h\nu$ incident from the left strikes an electron bound to an atom with binding energy E_b. The photon vanishes, giving a kinetic energy of $T = h\nu - E_b$ to the electron, which departs at angle θ relative to the incident photon's direction. To conserve momentum the remainder of the atom departs at an angle φ. The atom's kinetic energy T_a is practically zero.

cannot take place with respect to a given electron unless $h\nu > E_b$ for that electron. The smaller $h\nu$ is, the more likely is the occurrence of the photoelectric effect, so long as $h\nu > E_b$. The photon is totally absorbed in the interaction, and ceases to exist. The kinetic energy given to the electron, *independent of its scattering angle* θ, is

$$T = h\nu - E_b - T_a \tag{7.28}$$

$$= h\nu - E_b \tag{7.29}$$

The kinetic energy T_a given to the recoiling atom is nearly zero,* justifying the conventional use of an equality sign rather than an approximation sign in Eq. (7.29).

The electron departs from the interaction at an angle θ relative to the photon's direction of incidence, carrying momentum p. Since the photon has been totally absorbed, it provides no scattered photon to assist in conserving momentum, as in the Compton effect case. In the photoelectric effect that role is assumed by the atom from which the electron was removed. Although its kinetic energy $T_a \cong 0$, its momentum p_a cannot be negligible. The direction taken by the recoiling atom is of little consequence, since it carries negligible kinetic energy. Suffice it to say that the atom scatters in the direction required to conserve momentum in each photoelectric event, and that $0 < \varphi < 180°$.

B. Interaction Cross Section for the Photoelectric Effect

Theoretical derivation of the interaction cross section for the photoelectric effect is more difficult than for the Compton effect, because of the complications arising from the binding of the electron. There is no simple equation for the differential photoelectric cross section that corresponds to the K-N formula. However, satisfactory solutions have been reported by different authors for several photon energy regions, as discussed by Evans (1955) and more recently by Hubbell (1969). Published tables of photoelectric interaction coefficients such as those in the latter reference are based on experimental results, supplemented by theoretically assisted interpolations for other energies and absorbing media than those measured.

The directional distribution of photoelectrons per unit solid angle is shown in Fig. 7.11. These are theoretical results from a review by Davisson and Evans (1952). The photoelectrons are seen to be ejected predominately sideways for low photon energies, because they tend to be emitted in the direction of the photon's electric vector. With increasing photon energy this distribution gets pushed more and more toward smaller (but still nonzero) angles. Electron scattering at 0° is forbidden because that is perpendicular to the electric vector.

A summary representation of the angular distribution of photoelectrons is conveyed by the bipartition angle shown in Fig. 7.12. One-half of all the photoelectrons are ejected at angles θ less than the bipartition angle. For example, photons of 0.5

* $T_a/T = m_0/M_0$, where m_0 is the rest mass of the electron and M_0 that of the recoiling atom. For example, an atom of ^{27}Al would carry approximately 0.002% as much kinetic energy as the photoelectron. Heavier atoms would carry even less.

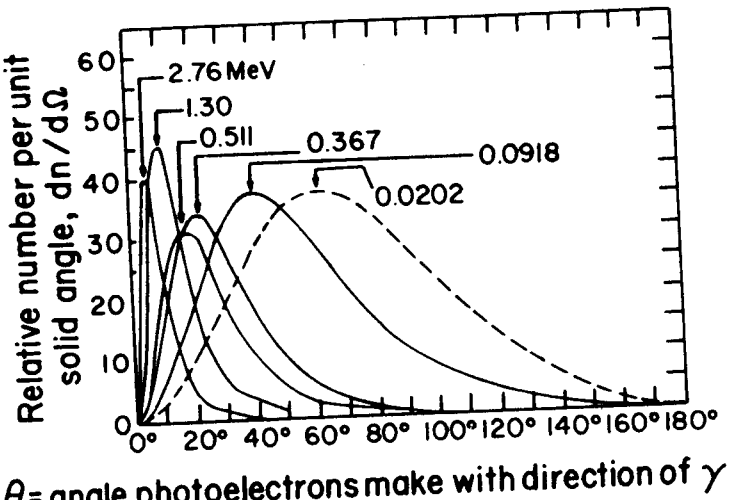

FIGURE 7.11. Directional distribution of photoelectrons per unit solid angle, for energies as labeled on the curves. The curve areas are not normalized to each other. [After Davisson and Evans (1952). Reproduced with permission of R. D. Evans and the American Physical Society.]

MeV send out half of their photoelectrons within a forward cone of half angle $\cong 30°$, and the remainder at larger angles.

The interaction cross section per atom for photoelectric effect, integrated over all angles of photoelectron emission, can be written as

$$_a\tau \cong k\frac{Z^n}{(h\nu)^m} \qquad (\text{cm}^2/\text{atom}) \tag{7.30}$$

where k is a constant,

$n \cong 4$ at $h\nu = 0.1$ MeV, gradually rising to about 4.6 at 3 MeV, and

$m \cong 3$ at $h\nu = 0.1$ MeV, gradually decreasing to about 1 at 5 MeV.

In the energy region $h\nu \cong 0.1$ MeV and below, where the photoelectric effect becomes most important, it is convenient to remember that

$$_a\tau \propto \frac{Z^4}{(h\nu)^3} \qquad (\text{cm}^2/\text{atom}) \tag{7.31}$$

and consequently that the photoelectric mass attenuation coefficient becomes [by employing the conversion factors in Eqs. (7.17) and (7.18)]

$$\frac{\tau}{\rho} \propto \left(\frac{Z}{h\nu}\right)^3 \qquad (\text{cm}^2/\text{g}) \tag{7.32}$$

This approximate relationship may be compared with the curves in Fig. 7.13,

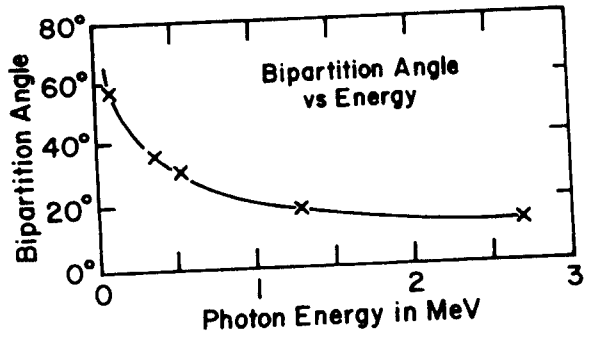

FIGURE 7.12. Bipartition angle of photoelectrons vs $h\nu$. One-half of all the photoelectrons are ejected within a forward cone of half angle equal to the bipartition angle. [After Davisson and Evans (1952). Reproduced with permission of R. D. Evans and the American Physical Society.]

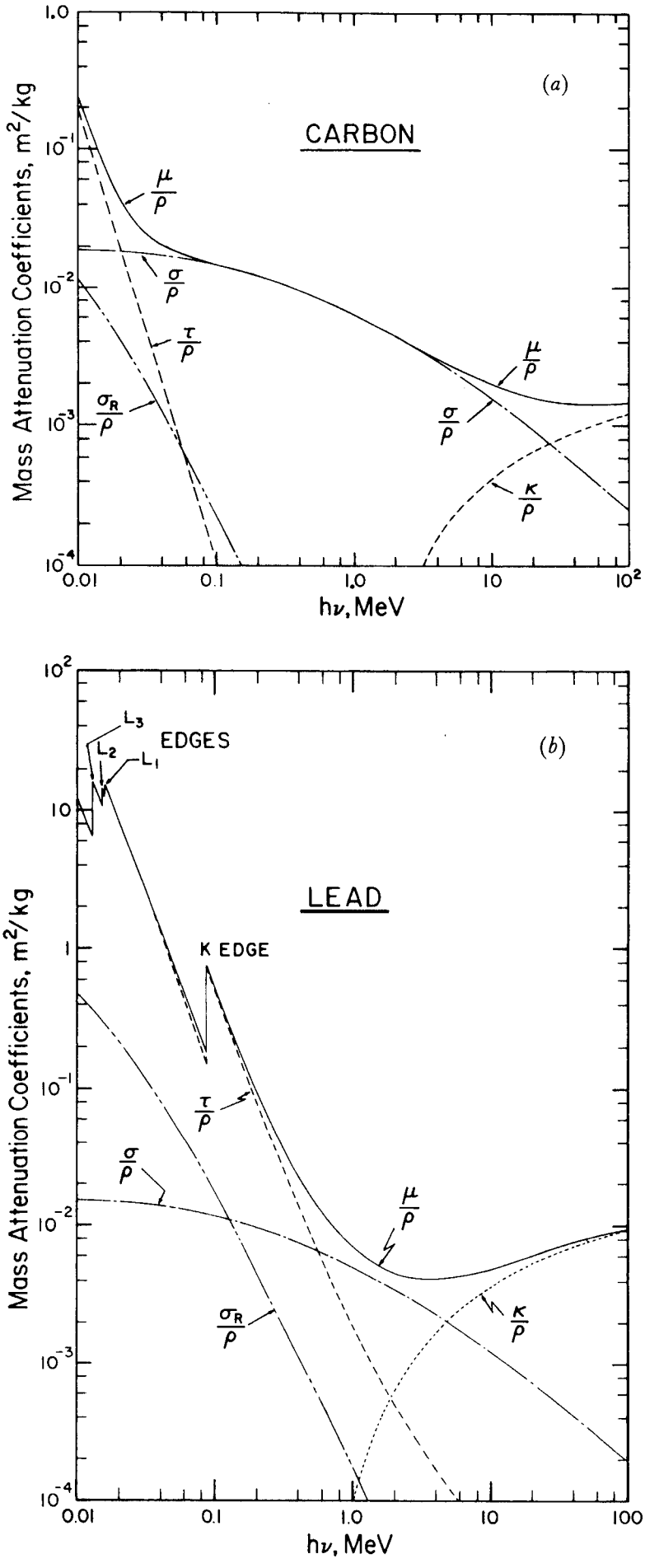

FIGURE 7.13. Mass attenuation coefficients for carbon (*a*) and lead (*b*). τ/ρ indicates the contribution of the photoelectric effect, σ/ρ is that of the Compton effect, κ/ρ that of pair production, and σ_R/ρ that of Rayleigh (coherent) scattering. μ/ρ is their sum, which is closely approximated in Pb by the τ/ρ curve below $h\nu = 0.1$ MeV (From data of Hubbell, 1969).

derived from empirically based tabulated values. The curve labeled τ/ρ in part *a* represents the photoelectric mass attenuation coefficient for carbon, and in part *b* that for lead, plotted vs. $h\nu$. The carbon curve clearly approximates the $(h\nu)^{-3}$ dependence; the lead does likewise except where the breaks occur. Below the so-called "*K*-edge" at 88 keV, the two K-shell electrons cannot participate in the photoelectric effect because their binding energy $(E_b)_K = 88$ keV is too great. Only the *L*, *M*, and higher-shell electrons can do so. Just above 88 keV the *K*-electrons can also participate. Thus the magnitude of the resulting step function (from 7.1 down to 1.7 cm^2/g) indicates the importance of the contribution of the two *K*-shell electrons to the photoelectric cross section, in comparison with the other 80 electrons in the atom. The *K*-shell contributes over three-fourths, because of the large binding energy of those two electrons and the strong dependence of the photoelectric effect upon binding energy. The *L*-shell shows a similar effect at the three *L* edges (L_1 at 15.9, L_2 at 15.2, and L_3 at 13.0 keV) which correspond to the three energy levels in the *L* shell. The combined *L*-edge step is smaller than that at the *K*-edge, because of the lower *L*-shell binding energies.

Referring again to Fig. 7.13, it can also be seen that the (τ/ρ) curve in lead is roughly three decades higher than that in carbon in the low-energy region, as predicted by Eq. (7.32), since $Z_{Pb} = 82$ is of the order of 10 times greater than $Z_C = 6$.

C. Energy-Transfer Cross Section for the Photoelectric Effect

It is evident from the conservation-of-energy equation (7.29) for the photoelectric effect that the fraction of $h\nu$ that is transferred to the photoelectron is simply

$$\frac{T}{h\nu} = \frac{h\nu - E_b}{h\nu} \tag{7.33}$$

However, this is only a first approximation to the total fraction of $h\nu$ that is transferred to all electrons. The binding energy E_b must be taken into account, and part or all of it is converted into electron kinetic energy through the *Auger effect*, to be considered next.

When an electron is removed from an inner atomic shell by any process, such as the photoelectric effect, internal conversion, electron capture, or charged-particle collision, the resulting vacancy is promptly filled by another electron falling from a less tightly bound shell. For *K*- and *L*-shell vacancies this transition is sometimes accompanied by the emission of a fluorescence x-ray of quantum energy $h\nu_K$ or $h\nu_L$, respectively, equal to the difference in potential energy between the donor and recipient levels, as discussed in Chapter 9, Section II.A. The probability of this happening is called the *fluorescence yield*, Y_K or Y_L, respectively; values are plotted in Fig. 7.14 as a function of atomic number. Y_K is seen to rise rapidly for $Z > 10$, gradually approaching unity for high-*Z* elements, while Y_L is practically zero below copper, rising to only 0.42 at $Z = 90$. The chance of fluorescence x-ray emission during the filling of a vacancy in the *M* (or higher) shell is negligibly small.

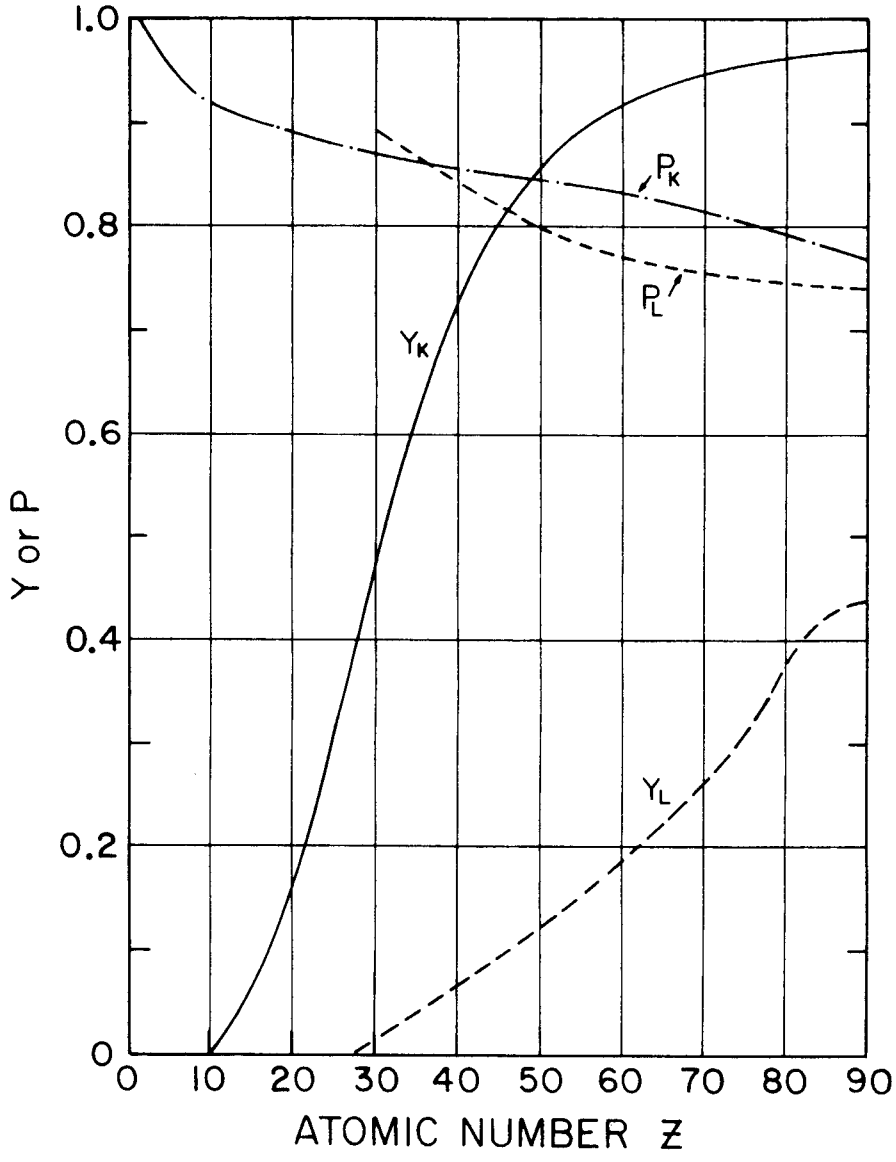

FIGURE 7.14. Fluorescence yield ($Y_{K,L}$) and fractional participation in the photoelectric effect ($P_{K,L}$) by K- and L-shell electrons (see text). P_K and P_L was calculated from tables of Hubbell (1969) and McMaster et al. (1969); Y_K from Lederer and Shirley (1979); and Y_L from Burhop (1952).

The role of the Auger effect is to provide an alternative mechanism by which the atom can dispose of whatever part of the binding energy E_b is not removed by a fluorescence x-ray. If no x-ray is emitted, then all of E_b is disposed of by the Auger process. In the Auger effect the atom ejects one or more of its electrons with sufficient kinetic energy to account collectively for the excess energy. Thus any energy invested in such Auger electrons contributes to the kerma.

An atom may emit a number of Auger electrons more or less simultaneously in a kind of chain reaction. The atom thus exchanges one energetically "deep" inner-shell vacancy for a number of relatively shallow outer-shell vacancies. These vacancies are finally neutralized by conduction-band electrons.

The energy budget in the Auger effect is illustrated in the following example: Suppose a K-shell vacancy appears, with binding energy $(E_b)_K$. Assume that an electron falls in from the L-shell, as is most often the case. Letting the binding energy

in that shell be $(E_b)_L$, either the atom will emit an x-ray of energy $h\nu_K = (E_b)_K - (E_b)_L$, or it must dispose of that energy [as well as the remaining energy $(E_b)_K - h\nu_K$] through the Auger effect. (Notice that for intuitive convenience we are treating the binding energies as positive potentials, whereas they are actually negative.) Assuming that the atom opts entirely for the Auger effect, it may eject an electron from any shell outside of that in which the original vacancy occurred, in this case the K-shell. If an M-shell electron is ejected, it will have a kinetic energy T_M equal to

$$T_M = (E_b)_K - (E_b)_L - (E_b)_M \tag{7.34a}$$

where $(E_b)_M$ is the binding energy in the M shell.

Now the atom has two electron vacancies, one in the L- and one in the M-shell. Let us assume that two N-shell electrons move in to fill those vacancies, and that the atom emits two more Auger electrons. If they both happened to be ejected from the N-shell, the atom would then have *four* N-shell vacancies. One of the those Auger electrons would have the kinetic energy

$$T_{N1} = (E_b)_L - 2(E_b)_N \tag{7.34b}$$

and the other would have

$$T_{N2} = (E_b)_M - 2(E_b)_N \tag{7.34c}$$

Thus the total kinetic energy of the three Auger electrons generated so far would be equal to

$$T_A = T_M + T_{N1} + T_{N2} = (E_b)_K - 4(E_b)_N \tag{7.34d}$$

This process is repeated, increasing the number of electron vacancies by one for each Auger event that occurs, until all the vacancies are located in the outermost shell(s). The total amount of kinetic energy carried by all the Auger electrons together is equal to the original-shell binding energy $(E_b)_K$ minus the sum of the binding energies of all the final electron vacancies. As these are subsequently neutralized by electrons from the conduction band, those electrons as they approach will acquire kinetic energies equal to the outer-shell binding energies of the vacancies they fill. Thus *all* of $(E_b)_K$ in this example ends up as electron kinetic energy, contributing to the kerma. If an x-ray $h\nu_K$ had been emitted, then the remainder of $(E_b)_K$ would have become electron kinetic energy.

It should be mentioned that since an Auger chain reaction or "shower" suddenly produces a multiply charged ion, which may have a net positive charge even in excess of 10 elementary charges, the resulting local Coulomb-force field can be quite disruptive to its molecular or crystalline surroundings.

Returning now to consideration of fluorescence x-rays, it is shown in Chapter 9, Section II.A, that there are several levels in the L or higher shells from which the K-shell replacement electron may come, although some specific transitions are quantum-mechanically forbidden to occur. As a result $h\nu_K$ has several closely grouped values that may be represented for present purposes by a mean value $h\bar{\nu}_K$. Figure

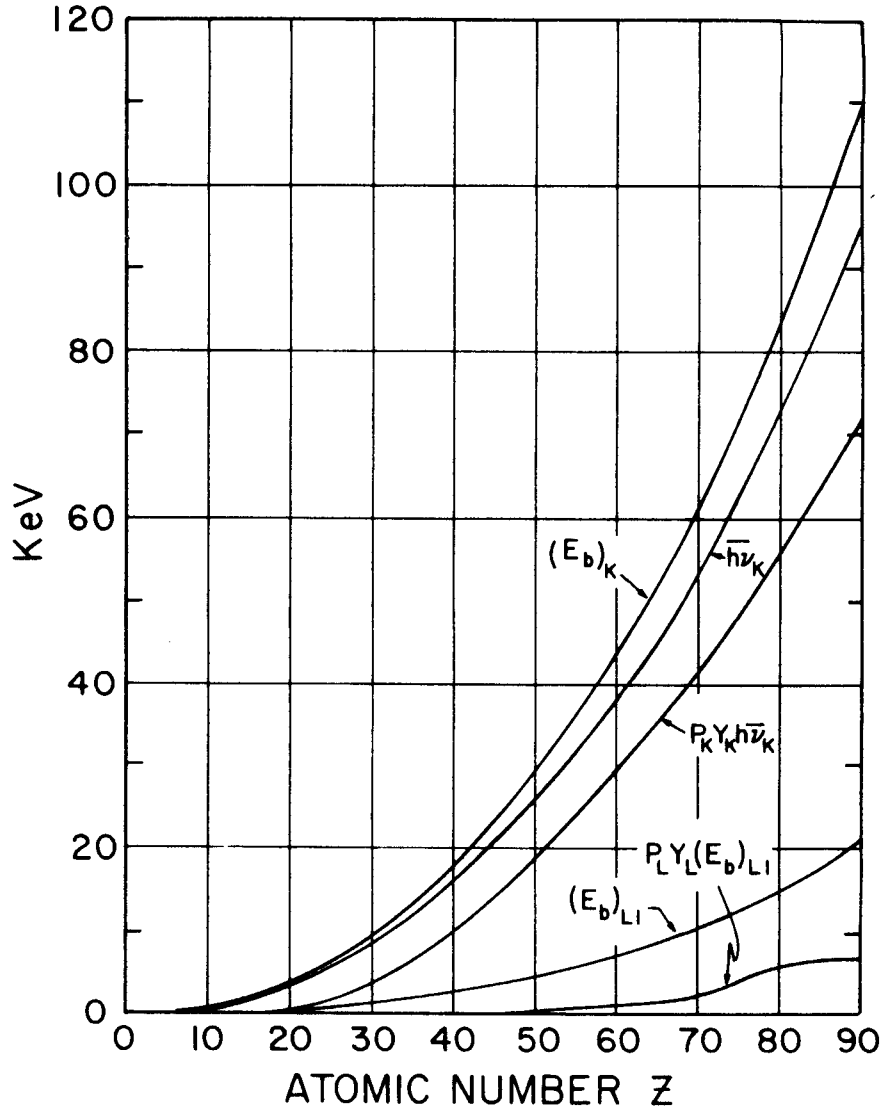

FIGURE 7.15. Electron binding energies $(E_b)_K$ in the K-shell and $(E_b)_{L1}$ in the $L1$-shell; weighted mean fluorescence x-ray energy $h\bar{\nu}_K$ in the K-shell; and the products $P_K Y_K \cdot h\bar{\nu}_K$ and $P_L Y_L\ (E_b)_{L1}$. The latter provides an upper-limit estimate of $P_L Y_L\, h\bar{\nu}_L$. Taken or derived from tables by Lederer and Shirley (1979).

7.15 contains a graph of $h\bar{\nu}_K$ vs. Z, which may be compared with the uppermost curve of K-shell binding energy $(E_b)_K$. Naturally $h\bar{\nu}_K < (E_b)_K$, because $(E_b)_K$ represents the difference in potential energy between an electron in the K-shell and one completely away from the atom, while fluorescence photons result from smaller transitions.

In addition to the fluorescence yields, Fig. 7.14 contains a second kind of function: P_K is the fraction (τ_K/τ) of all photoelectric interactions that occur in the K-shell, for photons for which $h\nu > (E_b)_K$. (This is the fraction obtainable from the height of the K-edge step, as mentioned earlier in relation to Fig. 7.13*b*). Likewise $P_L = \tau_L/\tau$ for photons where $(E_b)_{L1} < h\nu < (E_b)_K$. The product $P_K Y_K$ then is the fraction of all photoelectric events in which a K-fluorescence x-ray is emitted by the atom, and $P_L Y_L$ is the corresponding quantity for the L-shell, for the appropriate ranges of $h\nu$. The product $P_K Y_K \cdot h\bar{\nu}_K$ then represents the mean energy carried away from the atom by K-fluorescence x-rays, per photoelectric interaction in all shells combined, where

$h\nu > (E)_K$. An upper limit of a similar L-shell quantity $P_L Y_L \cdot h\bar{\nu}_L$ can be estimated as $P_L Y_L (E_b)_{L1}$. Both of these quantities are plotted in Fig. 7.15, and their use will be shown in subsequent discussion.

The probability of any other fluorescence x-ray except those from the K-shell being able to carry energy out of an atom is negligible for $h\nu > (E_b)_K$. For that case all the rest of the binding energy $(E_b)_K$, and all of the binding energy involved in photoelectric interactions in other shells, may be assumed to be given to Auger electrons. Thus we can write for the mean energy transferred to charged particles per photoelectric event

$$h\nu - P_K Y_K \cdot h\bar{\nu}_K \tag{7.35}$$

The photoelectric mass energy-transfer coefficient is thus given by

$$\frac{\tau_{tr}}{\rho} = \frac{\tau}{\rho}\left[\frac{h\nu - P_K Y_K h\bar{\nu}_K - (1 - P_K) P_L Y_L h\bar{\nu}_L}{h\nu}\right] \tag{7.36a}$$

for $h\nu > (E_b)_K$.

For photons having energies lying between the K and the highest L edge, [i.e., $(E_b)_{L1} < h\nu < (E_b)_K$], the corresponding equation for τ_{tr}/ρ can be written as

$$\frac{\tau_{tr}}{\rho} = \frac{\tau}{\rho}\left[\frac{h\nu - P_L Y_L \cdot h\bar{\nu}_L}{h\nu}\right] \tag{7.36b}$$

where $P_L Y_L \cdot h\bar{\nu}_L$ can be approximated by $P_L Y_L (E_b)_{L1}$, as plotted in Fig. 7.15; this quantity is insignificant except in high-Z materials.

It should be noted that even though fluorescence x-rays may carry some energy out of the atom of their origin, the distance that such an x-ray can penetrate through the medium before undergoing another photoelectric interaction will be severely limited. For example, the K-fluorescence from lead averages $\cong 76$ keV, for which the mass energy-absorption coefficient in lead is $\cong 0.23$ m^2/kg, and the broad-beam 10th-value layer is about 1 mm. For L fluorescence the photon penetration distance in lead is of the order of $\frac{1}{100}$ as great.

Figure 7.16 shows the mass energy-transfer coefficients for carbon and lead, corresponding to the attenuation coefficients shown in Fig. 7.13. Notice that the curve for $(\mu_{tr}/\rho)_{Pb}$ is practically equal to $(\tau_{tr}/\rho)_{Pb}$ for $h\nu \lesssim 0.1$ MeV, and that the size of the K-edge step is somewhat less here than in Fig. 7.13, due to the loss of K-fluorescence energy as indicated by Eq. (7.36a).

IV. PAIR PRODUCTION

Pair production is an absorption process in which a photon disappears and gives rise to an electron and a positron. It can only occur in a Coulomb force field, usually that near an atomic nucleus. However it can also take place, with lower probability, in the field of an atomic electron. This latter process is usually called "triplet production," because the host electron that provides the Coulomb field also acquires significant kinetic energy in conserving momentum. Thus two electrons and a positron are ejected from the site of the interaction. A minimum photon energy of $2m_0c^2$

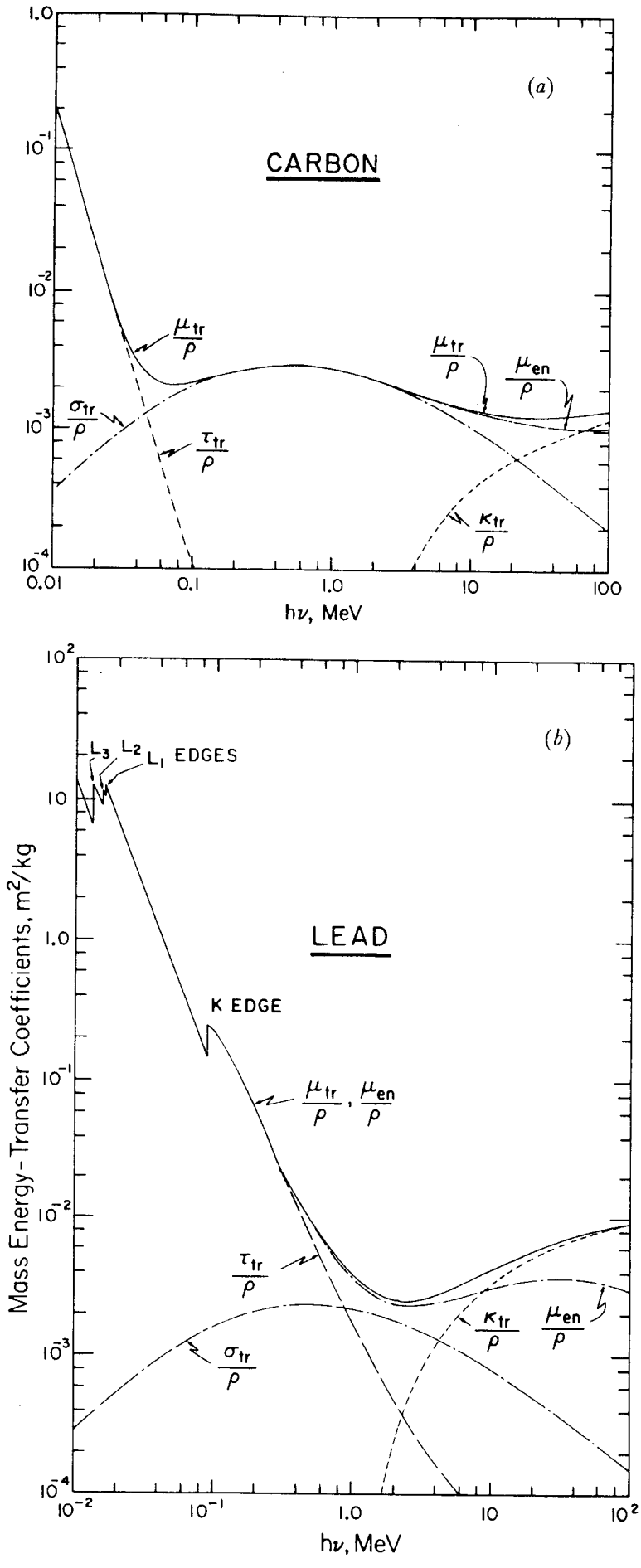

FIGURE 7.16. Mass energy-transfer coefficients for carbon (*a*) and lead (*b*). τ_{tr}/ρ indicates the contribution of the photoelectric effect, σ_{tr}/ρ that of the Compton effect, and κ_{tr}/ρ that of pair production. μ_{tr}/ρ represents their sum. The total mass energy-absorption coefficient (μ_{en}/ρ) is also shown. Note that these μ_{en}/ρ data for $h\nu > 10$ MeV do not take into account in-flight annihilation. Data after Hubbell (1969).

$= 1.022$ MeV is obviously required for pair production to occur in the nuclear field. $4m_0c^2$ is the threshold for triplet production, because of momentum-conservation considerations to be discussed later.

A. Pair Production in the Nuclear Coulomb Force Field

Figure 7.17 illustrates schematically a pair-production event in a nuclear field. The incident photon $h\nu$ gives up all of its quantum energy in the creation of the electron-positron pair with kinetic energies T^- and T^+. The energy-conservation equation, ignoring the vanishingly small kinetic energy given to the nucleus, is simply

$$\begin{aligned} h\nu &= 2m_0c^2 + T^- + T^+ \\ &= 1.022 \text{ MeV} + T^- + T^+ \end{aligned} \tag{7.37}$$

The electron and positron do not necessarily receive equal kinetic energies, but their average is given by

$$\overline{T} = \frac{h\nu - 1.022 \text{ MeV}}{2} \tag{7.38}$$

For $h\nu$ values well above the threshold energy $2m_0c^2$, the electrons and positrons are strongly forward directed. Their average angle of departure relative to the original photon direction is roughly

$$\bar{\theta} \cong \frac{m_0c^2}{\overline{T}} \qquad \text{(radians)} \tag{7.39}$$

For example, for $h\nu = 5$ MeV, we have $\overline{T} = 1.989$ MeV and $\bar{\theta} \cong 0.26$ radians $= 15°$.

From a theory due to Bethe and Heitler, the atomic differential cross section $d({}_a\kappa)$ for the creation of a positron of energy T^+ (and a corresponding electron of energy $h\nu - 2m_0c^2 - T^+$) is given by

$$d({}_a\kappa) = \frac{\sigma_0 Z^2 P}{h\nu - 2m_0c^2}\, dT^+ \qquad (\text{cm}^2/\text{atom}) \tag{7.40}$$

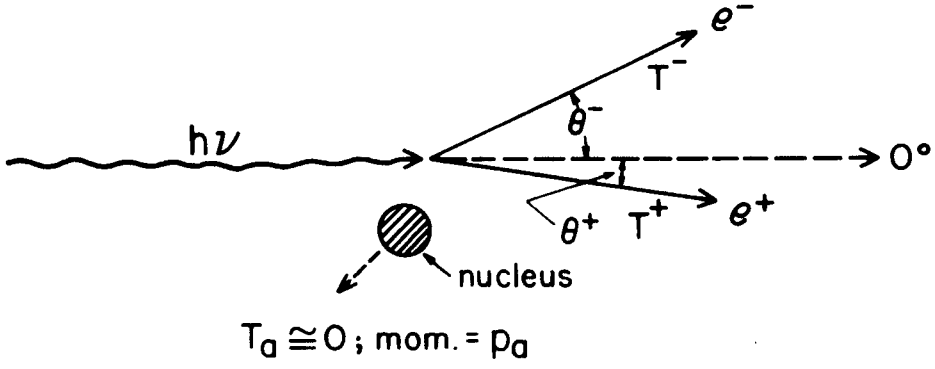

FIGURE 7.17. Pair production in the Coulomb force field of an atomic nucleus. An incident photon of quantum energy $h\nu$ vanishes, giving rise to a positron-electron pair. The atom participates in conservation of momentum, but receives negligible kinetic energy $T_a \cong 0$.

where

$$\sigma_0 = \frac{r_0^2}{137} = \frac{1}{137}\left(\frac{e^2}{m_0c^2}\right)^2 = 5.80 \times 10^{-28}\ \text{cm}^2/\text{electron},$$

and parameter P is a function of $h\nu$ and Z. P is displayed graphically in Figure 7.18 as a function of the fraction of the total kinetic energy that resides with the positron. A slight expected asymmetry in energy distributions between the positron and electron was neglected in deriving these P-values, which thus appear symmetrical about $T^+/(h\nu - 2m_0c^2) = 0.5$. Nuclear attraction and repulsion tend to give the positron slightly more energy than the electron, the difference being less than $0.0075Z$ MeV (Evans, 1955).

The total nuclear pair-production cross section per atom may be gotten by integrating $d({}_a\kappa)$ from Eq. (7.40) over all values of T^+:

$$\begin{aligned} {}_a\kappa &= \int_{T^+} d({}_a\kappa) = \sigma_0 Z^2 \int_0^{(h\nu - 2m_0c^2)} \frac{P\,dT^+}{h\nu - 2m_0c^2} \\ &= \sigma_0 Z^2 \int_0^1 P\,d\left(\frac{T^+}{h\nu - 2m_0c^2}\right) = \sigma_0 Z^2 \overline{P} \end{aligned} \tag{7.41}$$

Evidently ${}_a\kappa$ is proportional to the atomic number squared. The dependence of ${}_a\kappa$ upon $h\nu$ is roughly logarithmic through the $\overline{P}$-term, tending to become a constant

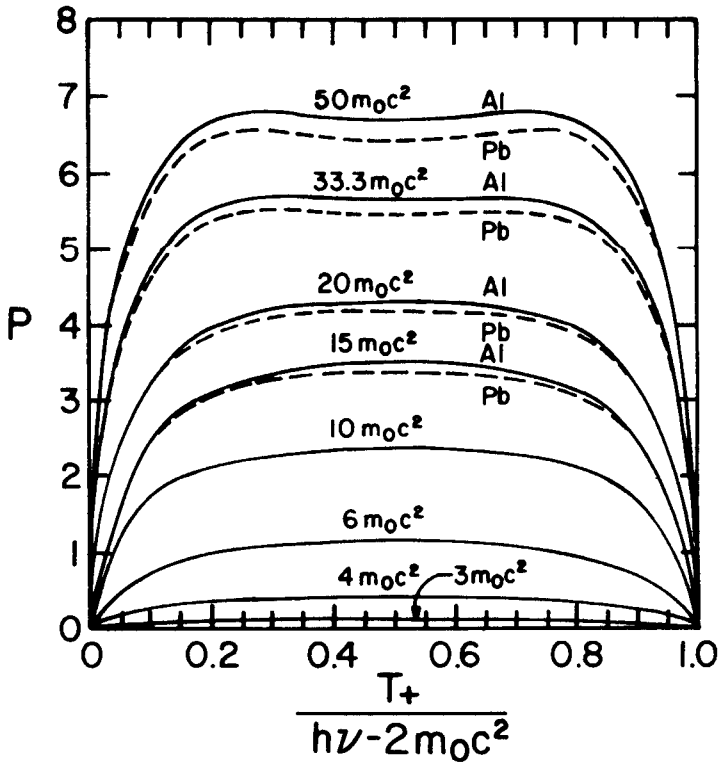

FIGURE 7.18. The quantity P in Eq. (7.41), plotted as a function of the kinetic-energy fraction given to the positron. The small difference between lead and aluminum shows the small amount of Z-dependence. [After Davisson and Evans (1952). Reproduced with permission of R. D. Evans and the American Physical Society.]

independent of $h\nu$ for very large $h\nu$ because of electron screening of the nuclear field (see Fig. 7.13).

The mass attenuation coefficient for nuclear pair-production is obtained from Eq. (7.41) as

$$\frac{\kappa}{\rho} = {}_a\kappa \frac{N_A}{A} \qquad (\text{cm}^2/\text{g}) \tag{7.42}$$

Again, since Z/A is roughly constant ($= 0.45 \pm 0.05$) except for hydrogen, $\kappa/\rho \approx Z$.

B. Pair Production in the Electron Field

In the kinematics of pair production in the electron field (i.e., triplet production), the photon divides its energy between the positron-electron pair produced and the host electron. The energy conservation equation becomes

$$h\nu = 1.022 \text{ MeV} + T^+ + T_1^- + T_2^- \tag{7.43}$$

and the average kinetic energy of the three particles is

$$\overline{T} = \frac{h\nu - 1.022 \text{ MeV}}{3} \tag{7.44}$$

As mentioned earlier, the threshold for this process is $4m_0c^2 = 2.044$ MeV, even though the energy being converted into mass is still $2m_0c^2$, the same as for nuclear-field pair production. It can be shown, as follows, that the higher threshold is required by conservation of momentum, as first derived by Perrin (1933).

In Fig. 7.19*a* a photon of energy $h\nu$ is shown approaching an electron e_1^- assumed to be at rest in the laboratory frame of reference, R. For convenience the same two particles are considered in Fig. 7.19*b* with respect to a moving frame of reference R', in which the momentum of the photon-electron system is null. The velocity of R' relative to R is $+\beta c$, that is, R' moves to the right with constant velocity. This makes the electron appear to move to the left with the same speed, i.e., $v = -\beta c$.

The resulting momentum of the electron is $-m\beta c = -m_0\beta c/\sqrt{1 - \beta^2}$, where m is the electron's relativistic mass with respect to R'. The photon's momentum relative to R' is $h\nu'/c$. Thus for null momentum we can write

$$\frac{h\nu'}{c} - \frac{m_0\beta c}{\sqrt{1 - \beta^2}} = 0 \tag{7.45}$$

The Doppler effect causes the frequency ν' of the photon relative to the moving frame of reference to be less than ν, according to the relation

$$\nu' = \nu \sqrt{\frac{1 - \beta}{1 + \beta}} \tag{7.46}$$

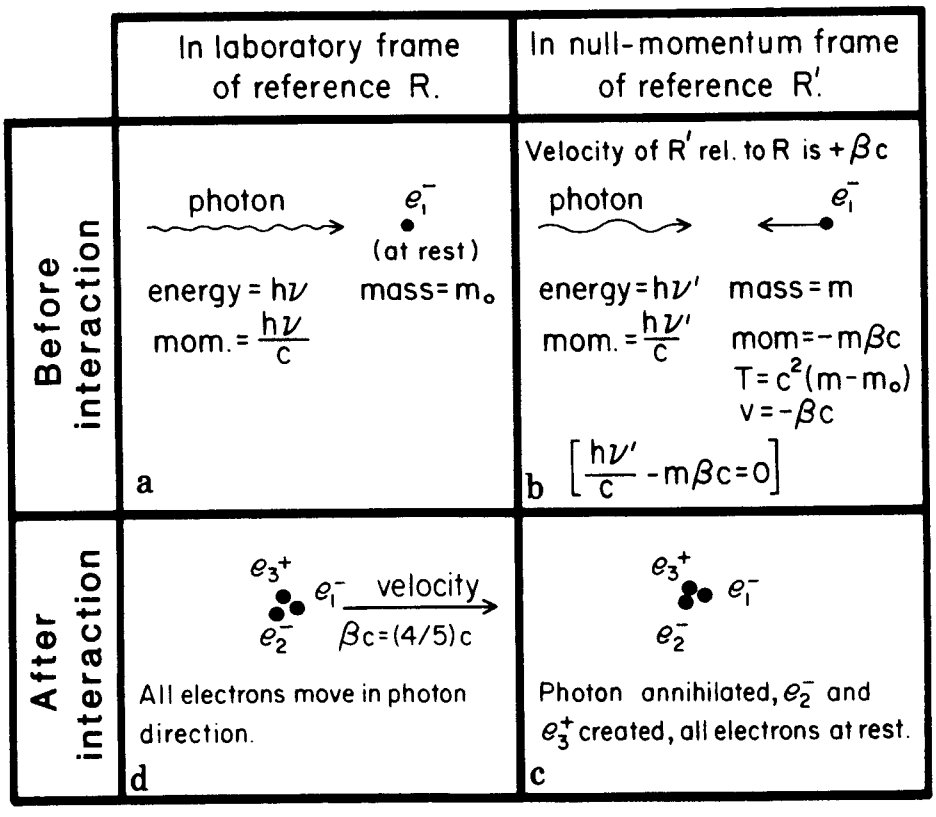

FIGURE 7.19. Triplet-production kinematics at the minimum photon energy threshold, $h\nu = h\nu_{min}$. Diagrams at left apply to the laboratory frame of reference R, those at right to moving frame of reference R'. The momentum of the photon-electron system is zero in R'.

Substitution of Eq. (7.46) to eliminate ν' in Eq. (7.45) allows solution for β:

$$\beta = \frac{\alpha}{1 + \alpha} \tag{7.47}$$

in which

$$\alpha \equiv \frac{h\nu}{m_0c^2} \tag{7.48}$$

The minimum photon energy, $h\nu_{min}$, necessary for triplet production can be derived by noting that the sum of the photon energy $h\nu'_{min}$ and the electron kinetic energy T relative to R' must just equal the total rest mass of the electron and positron created. That is,

$$h\nu'_{min} + m_0c^2\left(\frac{1}{\sqrt{1 - \beta_{min}^2}} - 1\right) = 2m_0c^2 \tag{7.49}$$

where

$$h\nu'_{min} = h\nu_{min}\sqrt{\frac{1 - \beta_{min}}{1 + \beta_{min}}}, \qquad \beta_{min} = \frac{\alpha_{min}}{1 + \alpha_{min}}, \qquad \alpha_{min} \equiv \frac{h\nu_{min}}{m_0c^2}$$

This equation can be solved for $\beta_{\min}$, which is found to have the value $\frac{4}{5}$. Thus $h\nu_{\min} = 4m_0c^2$.

It is interesting to observe that, in the moving frame of reference R', the two electrons and the positron all must be at rest after a minimum-$h\nu$ event, as shown in Fig. 7.19*c*. This is so because all of the available quantum and kinetic energy has been spent in mass creation, leaving none for motion. As a consequence, in the laboratory frame of reference all three particles in the triplet move together in the original photon's direction with velocity $(\beta c)_{\min} = \frac{4}{5}c$, as shown in Fig. 7.19*d*.

For higher incident photon energy than $4m_0c^2$ the three particles may share the excess energy and depart the point of the interaction in various directions, so long as the null momentum is preserved relative to R'. Perrin has shown that the kinetic energy of each of the particles, relative to the laboratory system, lies within the limits given by

$$T = \frac{\alpha^2 - 2\alpha - 2 \pm \alpha\sqrt{\alpha(\alpha - 4)}}{2\alpha + 1} \tag{7.50}$$

This reduces to $2m_0c^2/3$ for the threshold case in which $\alpha = 4$, meaning that the particles in Fig. 7.19*d* each have a kinetic energy equal to $\frac{1}{3}$ of the $2m_0c^2$ energy not needed for mass creation. For 10-MeV photons Eq. (7.50) predicts that the product particles each have energies between 3 keV and 8.7 MeV.

The atomic cross section for triplet production (i.e., for all the atomic electrons combined) is small compared to the nuclear pair-production cross section for the same atom. The ratio is given approximately by

$$\frac{{}_a\kappa(\text{electrons})}{{}_a\kappa(\text{nucleus})} \cong \frac{1}{CZ} \tag{7.51}$$

in which C is a parameter depending only on $h\nu$. C is unity for $h\nu \to \infty$, and rises slowly with decreasing energy to $\cong 2$ at 5 MeV (see discussion given by Evans, 1955). Thus in Pb the triplet cross section is only 1% or so of the pair-production cross section, rising to 5–10% for $Z = 10$.

For most purposes in radiological physics and dosimetry it will suffice to combine the separate cross sections for pair and triplet production into a single cross section for both, usually still called the pair-production cross section. Thus

$$\left(\frac{\kappa}{\rho}\right)_{\text{pair}} = \left(\frac{\kappa}{\rho}\right)_{\text{nuclear}} + \left(\frac{\kappa}{\rho}\right)_{\text{electron}} \tag{7.52}$$

C. Pair-Production Energy-Transfer Coefficient

The fraction of the incident photon's energy that is transferred to the kinetic energy of the charged particles, both for nuclear and electron pair production, is $(h\nu - 2m_0c^2)/h\nu$. Therefore the mass energy-transfer coefficient for pair production is given by

$$\frac{\kappa_{\text{tr}}}{\rho} = \frac{\kappa}{\rho}\left(\frac{h\nu - 2m_0c^2}{h\nu}\right) \tag{7.53}$$

V. RAYLEIGH (COHERENT) SCATTERING

Rayleigh scattering is called "coherent" because the photon is scattered by the combined action of the whole atom. The event is elastic in the sense that the photon loses essentially none of its energy; the atom moves just enough to conserve momentum. The photon is usually redirected through only a small angle. Therefore the effect on a photon beam can only be detected in narrow-beam geometry. Rayleigh scattering contributes nothing to kerma or dose, since no energy is given to any charged particle, nor is any ionization or excitation produced.

The photon scattering angle depends on both Z and $h\nu$: $\frac{2}{3}$ of the photons are scattered at angles smaller than these, according to Fano (1953a):

$h\nu$	$h\nu$ = 0.1 MeV	1 MeV	10 MeV
Al	15°	2°	0.5°
Pb	30°	4°	1.0°

It is seen that Rayleigh scattering has more practical importance at low energies, partly because the scattering angle is greater.

The atomic cross section for Rayleigh scattering is given by

$$ {}_a\sigma_R \propto \frac{Z^2}{(h\nu)^2} \qquad (\text{cm}^2/\text{atom}) \tag{7.54}$$

or in mass units

$$ \frac{\sigma_R}{\rho} \propto \frac{Z}{(h\nu)^2} \qquad (\text{cm}^2/\text{g or m}^2/\text{kg}) \tag{7.55}$$

Typical ratios of Rayleigh to total attenuation coefficients (σ_R/μ) are shown in the following table, derived from the tables of Hubbell (1969):

Element	$h\nu$ = 0.01 MeV	0.1 MeV	1.0 MeV
C	0.07	0.02	0
Cu	0.006	0.08	0.007
Pb	0.03	0.03	0.03

The relative importance of Rayleigh scattering is seen to be fairly small, as it contributes only a few percent or less of the narrow-beam attenuation coefficient. Pronounced trends vs. Z and $h\nu$ tend to be obscured by variations in the competing interactions—photoelectric effect and Compton effect. However, for low Z (e.g., carbon) a gain is evident with decreasing photon energy.

The mass attenuation coefficient for Rayleigh scattering is shown in relation to the other interaction coefficients in Fig. 7.13. Rough agreement with Eq. (7.55) can be seen.

VI. PHOTONUCLEAR INTERACTIONS

In a photonuclear interaction an energetic photon (exceeding a few MeV) enters and excites a nucleus, which then emits a proton or neutron. (γ, p) events contribute directly to the kerma, but the relative amount remains less than 5% of that due to pair production. Thus it has been commonly neglected in dosimetry considerations.

(γ, n) interactions have greater practical importance because the neutrons thus produced may lead to problems in radiation protection. This is the case for clinical x-ray generators (Linacs, microtrons, betatrons) in which electrons are accelerated to 10 MeV or more. The x-ray beam will be slightly contaminated with neutrons, to a degree depending on accelerator energy and design. A 25-MV x-ray beam will usually have an order-of-magnitude greater neutron contamination than a 10-MV beam, because of the correspondingly greater (γ, n) interaction cross section. The biological consequences of these neutrons in a radiotherapy patient are probably negligible in comparison with the effects of the predominating photon beam. Nevertheless, as a precaution, governmental regulatory agencies are placing limitations on allowable neutron levels in radiotherapy x-ray beams.

The presence of (γ, n) neutrons must be taken into account in shielding design, especially since neutrons can escape through mazes much more readily than photons can. Moreover, neutrons can activate accelerator hardware, especially in the target region. Such hardware may require a time delay before approaching for service, and should always be monitored first for γ- and β-activity. Some low level of radioactivation may also occur in the body tissues of radiotherapy patients, due either to incident neutrons or to photonuclear interactions occurring in the body itself.

All of these consequences of (γ, n) interactions can be regarded as unwanted side effects of the use of higher-energy radiotherapy x-ray beams, offset by the increasingly favorable spatial distributions of dose in the body that can be achieved by such beams. Swanson (1979) has provided useful estimates of (γ, n) neutron production in accelerators. Anderson (1984) presents additional discussion of the relevant physics of photonuclear interactions.

VII. TOTAL COEFFICIENTS FOR ATTENUATION, ENERGY TRANSFER, AND ENERGY ABSORPTION

A. Mass Attenuation Coefficient

The total mass attenuation coefficient for γ-ray interactions, neglecting photonuclear interactions, can be written, in units of cm^2/g or m^2/kg, as

$$\frac{\mu}{\rho} = \frac{\tau}{\rho} + \frac{\sigma}{\rho} + \frac{\kappa}{\rho} + \frac{\sigma_R}{\rho} \tag{7.56}$$

in which τ/ρ is the contribution of the photoelectric effect, σ/ρ that of the Compton effect, κ/ρ that of pair production, and σ_R/ρ that of Rayleigh scattering.

For the practical application of Eq. (7.56) as a definition of the mass "narrow-beam" attenuation coefficient (see Chapter 3), it should be noted that the term $\sigma_R/$

ρ is appropriately included only where beam geometry allows the escape (i.e. non-detection) of the Rayleigh-scattered rays. Since this type of scattering usually deflects photons through only small angles, very narrow beam geometry is required to observe the effects of Rayleigh scattering.

B. Mass Energy-Transfer Coefficient

The total mass energy-transfer coefficient for γ-ray interactions, neglecting any (γ, p) photonuclear contribution, is given in units of cm^2/g or m^2/kg by

$$\frac{\mu_{tr}}{\rho} = \frac{\tau_{tr}}{\rho} + \frac{\sigma_{tr}}{\rho} + \frac{\kappa_{tr}}{\rho}$$

$$= \frac{\tau}{\rho}\left[\frac{h\nu - p_K Y_k h\bar{\nu}_K}{h\nu}\right] + \frac{\sigma}{\rho}\left[\frac{\overline{T}}{h\nu}\right] + \frac{\kappa}{\rho}\left[\frac{h\nu - 2m_0c^2}{h\nu}\right] \tag{7.57}$$

for photons having $h\nu$ above the K-edge in the elemental absorbing medium, and neglecting L-fluorescence in comparison with K-fluorescence. For $h\nu$ lying between the K- and L-edges, Eq. (7.57) is replaced by

$$\frac{\mu_{tr}}{\rho} = \frac{\tau_{tr}}{\rho} + \frac{\sigma_{tr}}{\rho}$$

$$= \frac{\tau}{\rho}\left[\frac{h\nu - p_L Y_L h\bar{\nu}_L}{h\nu}\right] + \frac{\sigma}{\rho}\left[\frac{\overline{T}}{h\nu}\right] \tag{7.58}$$

since neither K-fluorescence nor pair production is relevant in that case. The terms in Eqs. (7.57) and (7.58) have been defined in Eqs. (7.35) and (7.36) for the photoelectric effect, Eqs. (7.20), (7.22), and (7.24) for the Compton effect, and Eq. (7.53) for pair production.

C. Mass Energy-Absorption Coefficient

The mass energy-absorption coefficient μ_{en}/ρ is related to the mass energy-transfer coefficient by

$$\frac{\mu_{en}}{\rho} = \frac{\mu_{tr}}{\rho}(1 - g) \tag{7.59}$$

in which g represents the average fraction of secondary-electron energy that is lost in radiative interactions, that is, bremsstrahlung production and (for positrons) in-flight annihilation. The evaluation of g will be discussed in Chapter 8, Section I.G. For low values of Z and $h\nu$, g approaches zero and $\mu_{en}/\rho \cong \mu_{tr}/\rho$. For increasing Z or $h\nu$, g increases gradually, so that, for example, in Pb with $h\nu = 10$ MeV, $\mu_{en}/\rho = 0.74\,\mu_{tr}/\rho$.

It should be pointed out that, while μ/ρ and μ_{tr}/ρ are based only on the $h\nu$ and Z actually present at the point of photon interaction, μ_{en}/ρ must also be based on an assumption about the medium through which the secondary electrons pass in slowing down. Conventionally the interaction point is assumed to be surrounded

by the same homogenous medium, at least out to a distance equal to the maximum electron range. Thus g in Eq. (6.59) is evaluated for the same surrounding material as assumed for μ_{tr}/ρ. It is possible to conceive of situations (e.g. near an interface) where the radiation yield of the electrons would be altered and the conventional value of μ_{en}/ρ could no longer predict how much energy would be spent in ionization and excitation by the secondary electrons.

D. Coefficients for Compounds and Mixtures

For compounds or intimate mixtures of elements the Bragg rule conveniently applies to mass attenuation and energy-transfer coefficients:

$$\left(\frac{\mu}{\rho}\right)_{\text{mix}} = \left(\frac{\mu}{\rho}\right)_A f_A + \left(\frac{\mu}{\rho}\right)_B f_B + \cdots \tag{7.60}$$

and

$$\left(\frac{\mu_{tr}}{\rho}\right)_{\text{mix}} = \left(\frac{\mu_{tr}}{\rho}\right)_A f_A + \left(\frac{\mu_{tr}}{\rho}\right)_B f_B + \cdots \tag{7.61}$$

where $f_A, f_B, \ldots$, are the weight fractions of the separate elements (A, B, . . .) present.

This same rule also applies approximately to the mass energy-absorption coefficient, so long as radiative losses are small. That is,

$$\begin{aligned}\left(\frac{\mu_{en}}{\rho}\right)_{\text{mix}} &\cong \left(\frac{\mu_{en}}{\rho}\right)_A f_A + \left(\frac{\mu_{en}}{\rho}\right)_B f_B + \cdots \\ &\cong \left(\frac{\mu_{tr}}{\rho}\right)_A (1 - g_A) f_A + \left(\frac{\mu_{tr}}{\rho}\right)_B (1 - g_B) f_B + \cdots\end{aligned} \tag{7.62}$$

where the second statement is based on Eq. (7.59), and where g_A is the radiation yield fraction for element A, and so on.

Equation (7.62) would be exact if the electrons originating in atoms of element A confined their paths to traversing only other atoms of the same element. However, the electrons actually pass through the different elements present in proportion to their weight fractions. Thus we may write an exact equation to replace Eq. (7.62) by expanding the radiation-yield terms accordingly to give

$$\begin{aligned}\left(\frac{\mu_{en}}{\rho}\right)_{\text{mix}} = &\left(\frac{\mu_{tr}}{\rho}\right)_A (1 - f_A g_A - f_B g_B - \cdots) f_A \\ &+ \left(\frac{\mu_{tr}}{\rho}\right)_B (1 - f_A g_A - f_B g_B - \cdots) f_B + \cdots\end{aligned}$$

$$= \left(\frac{\mu_{tr}}{\rho}\right)_{mix} (1 - f_A g_A - f_B g_B - \cdots)$$

$$\equiv \left(\frac{\mu_{tr}}{\rho}\right)_{mix} (1 - g_{mix}) \tag{7.63}$$

Values of g_A, g_B, . . . can be obtained from tables of μ_{tr}/ρ and μ_{en}/ρ, together with Eq. (7.59).

E. Tables of Photon Interaction Coefficients

Appendix D.1 contains tables of K–N interaction and energy-transfer cross sections in units of cm^2/e, for the energy range 1 keV to 100 MeV. These data apply to the Compton effect in all media, assuming free electrons.

Appendix D.2 provides photon interaction cross sections per atom for several representative elements, compounds, and mixtures over the same energy range. Besides giving data for the photoelectric effect, Compton effect, pair production, and Rayleigh (coherent) scattering, their combined effect is given with and without Rayleigh scattering. Appendix D.3 tabulates mass attenuation coefficients μ/ρ, mass energy-transfer coefficients μ_{tr}/ρ, and mass energy absorption coefficients μ_{en}/ρ. The last have been corrected for radiative losses due to positron in-flight annihilation as well as bremsstrahlung. μ_{en}/ρ values for a few additional materials also are given in Appendix D.4.

There are several other available tables of photon interaction data that deserve mention here:

1. McMaster et al. (1969) give a compilation of individual interaction cross-section data for $Z = 1$ to 83, 86, 90, 92, and 94, with $h\nu$ covering the range 1 keV to 1 MeV. Total attenuation coefficients are also included.
2. Storm and Israel (1970) have provided a very useful table of atomic cross sections for $Z = 1$–100 and $h\nu = 1$ keV to 100 MeV. In our terminology their table columns give the photon energy E, ${}_a\sigma$, ${}_a\sigma_{en}$, ${}_a\sigma_R$, ${}_a\kappa$(nuclear), ${}_a\kappa$(electron), ${}_a\kappa_{en}$(nuclear) + ${}_a\kappa_{en}$(electron), ${}_a\tau$, ${}_a\tau_{en}$, ${}_a\mu$, ${}_a\mu - {}_a\sigma_s - {}_a\sigma_R$, and ${}_a\mu_{en}$. The Compton-effect cross sections include binding corrections, but positron in-flight annihilation is not accounted for in ${}_a\kappa_{en}$ or ${}_a\mu_{en}$. This reference also contains some other useful tables, including (a) atomic energy levels, (b) K- and L-fluorescent x-ray energies, (c) weighted-average K and L x-ray energies, (d) relative intensities of K and L x-rays, (e) theoretical vs. experimental photoelectric cross sections, and (f) relative shell contributions to photoelectric cross sections.
3. Hubbell et al. (1980) give tables of photon cross sections for all the individual interactions, for $h\nu = 1$ MeV to 100 GeV and $Z = 1$–100. Total attenuation coefficients are also given. The Compton effect includes electron binding corrections.
4. Hubbell (1982) updates all his previous compilations in abbreviated form, i.e., listing only μ/ρ and μ_{en}/ρ for 40 elements and 45 mixtures and compounds.

Several ICRP (1975) body compositions (blood, bone, brain, lung, skin, and soft-tissue) are included. In-flight annihilation is taken into account in μ_{en}/ρ up to $h\nu$ = 10 MeV, and extrapolated to 20 MeV.

PROBLEMS*

1. Is the mass Compton coefficient (either for attenuation or energy transfer) larger in carbon or lead? (See Figs. 7.13*a*, *b*, 7.16*a*, *b*.) Why?
2. Why is Rayleigh scattering not plotted in Fig. 7.16*a*, *b*, although quite significant in Fig. 7.13*a*, *b*?
3. On the basis of the K–N theory, what is the ratio of the Compton interaction cross sections per atom for lead and carbon?
4. Calculate the energy of the Compton-scattered photon at $\varphi = 0°$, 45°, 90°, and 180° for $h\nu$ = 50 keV, 500 keV, and 5 MeV.
5. What are the corresponding energies and angles of the recoiling electrons for the cases in problem 4?
6. Calculate for 1-MeV photons the total K–N cross section from Eq. (7.15), and derive the Compton mass attenuation coefficient for copper, expressed in cm^2/g and m^2/kg.
7. What is the maximum energy, and what is the average energy, of the Compton recoil electrons generated by 20-keV and 20-MeV γ-rays?
8. Calculate the energy of a photoelectron ejected from the *K*-shell in tin by a 40-keV photon. Calculate τ_{tr}/ρ; you may estimate from Fig. 7.15.
9. What is the average energy of the charged particles resulting from pair production in (a) the nuclear field and (b) the electron field, for photons of $h\nu$ = 2 and 20 MeV?
10. A narrow beam containing 10^{20} photons at 6 MeV impinges perpendicularly on a layer of lead 12 mm thick, having a density of 11.3 g/cm^3. How many interactions of each type (photoelectric, Compton, pair, Rayleigh) occur in the lead?
11. Assuming that each interaction in problem 10 results in one primary photon being removed from the beam, how much energy is removed by each type of interaction?
12. How much energy is transferred to charged particles by each type of interaction in problem 10?

SOLUTIONS TO PROBLEMS

1. Carbon, because of larger electron density ($N_A Z/A$).
2. Rayleigh scattering transfers no energy to charged particles.

*Refer to the Appendix tables for required coefficients.

3. 82/6, since all electrons are assumed to be unbound and to have the same interaction cross section.

4. At

$$\begin{aligned}\varphi = 0°&: h\nu' = h\nu;\\ 45°&: h\nu' = 0.0486,\ 0.389,\ 1.293\ \text{MeV};\\ 90°&: h\nu' = 0.0455,\ 0.253,\ 0.464\ \text{MeV};\\ 180°&: h\nu' = 0.0418;\ 0.169,\ 0.243\ \text{MeV}.\end{aligned}$$

Also compare with Fig. 7.3.

5. At $\theta = 90°$, $T = 0$ for all $h\nu$. For $h\nu = 0.05$ MeV, $T = 1.39 \times 10^{-3}$, 4.46×10^{-3}, and 8.18×10^{-3} MeV at $\theta = 65.5°$, 42.3°, and 0°, respectively. For $h\nu = 0.5$ MeV, $T = 0.111$, 0.247, and 0.331 MeV at $\theta = 50.7°$, 26.8° and 0°, respectively. For $h\nu = 5$ MeV, $T = 3.71$, 4.54, and 4.76 MeV at $\theta = 12.6°$, 5.30°, and 0°, respectively.

6. ${}_e\sigma = 2.112 \times 10^{-25}$ cm²/electron; $(\sigma/\rho)_{Cu} = 0.0580$ cm²/g = 0.00580 m²/kg.

7. At

$$\begin{aligned}20\ \text{keV}&: T_{max} = 1.45\ \text{keV}, \quad \overline{T} = 0.721\ \text{keV}\\ 20\ \text{MeV}&: T_{max} = 19.75\ \text{MeV}, \ \overline{T} = 14.5\ \text{MeV}\end{aligned}$$

8. $T = 10.8$ keV; $\tau_{tr}/\rho = 0.99$ m²/kg.

9. At

$$\begin{aligned}h\nu = 2\ \text{MeV}&: \ \overline{T} = 0.489,\ 0\ \text{MeV}.\\ h\nu = 20\ \text{MeV}&: \overline{T} = 9.49,\ 6.33\ \text{MeV}.\end{aligned}$$

10. Photoelectric: 1.00×10^{18}; Compton: 1.793×10^{19}; pair: 2.556×10^{19}, Rayleigh: $\cong 6 \times 10^{16}$.

11. Photoelectric: 9.6×10^{5} J; Compton: 1.72×10^{7} J; pair: 2.46×10^{7} J; Rayleigh: 6×10^{4} J.

12. Photoelectric: 9.5×10^{5} J; Compton: 1.11×10^{7} J; pair: 2.04×10^{7} J; Rayleigh: 0.